Biogeosciences, 21, 1135–1159, 2024
https://doi.org/10.5194/bg-21-1135-2024

Biogeosciences Open Access EGU

Insights into carbonate environmental conditions in the Chukchi Sea

Claudine Hauri[1], Brita Irving[1], Sam Dupont[2,3], Rémi Pagés[1], Donna D. W. Hauser[1], and Seth L. Danielson[4]

[1]International Arctic Research Center, University of Alaska Fairbanks, Fairbanks, AK 99775, USA
[2]Department of Biological and Environmental Sciences, University of Gothenburg, Fiskebäckskil 45178, Sweden
[3]Radioecology Laboratory, International Atomic Energy Agency Marine Environmental Laboratories, Monaco, Monaco
[4]College of Fisheries and Ocean Science, University of Alaska Fairbanks, Fairbanks, AK 99775, USA

Correspondence: Claudine Hauri (chauri@alaska.edu)

Received: 24 June 2023 – Discussion started: 11 July 2023
Revised: 26 January 2024 – Accepted: 29 January 2024 – Published: 8 March 2024

Abstract. Healthy Arctic marine ecosystems are essential to the food security and sovereignty, culture, and wellbeing of Indigenous Peoples in the Arctic. At the same time, Arctic marine ecosystems are highly susceptible to impacts of climate change and ocean acidification. While increasing ocean and air temperatures and melting sea ice act as direct stressors on the ecosystem, they also indirectly enhance ocean acidification, accelerating the associated changes in the inorganic carbon system. Yet, much is to be learned about the current state and variability of the inorganic carbon system in remote, high-latitude oceans. Here, we present time series (2016–2020) of pH and the partial pressure of carbon dioxide (pCO_2) from the northeast Chukchi Sea continental shelf. The Chukchi Ecosystem Observatory includes a suite of subsurface year-round moorings sited amid a biological hotspot that is characterized by high primary productivity and a rich benthic food web that in turn supports coastal Iñupiat, whales, ice seals, walrus (*Odobenus rosmarus*), and Arctic cod (*Boreogadus saida*). Our observations suggest that near-bottom waters (33 m depth, 13 m above the seafloor) are a high carbon dioxide and low pH and aragonite saturation state (Ω_{arag}) environment in summer and fall, when organic material from the highly productive summer remineralizes. During this time, Ω_{arag} can be as low as 0.4. In winter, when the site was covered by sea ice, pH was < 8 and Ω_{arag} remained undersaturated under the sea ice. There were only two short seasonal periods with relatively higher pH and Ω_{arag}, which we term ocean acidification relaxation events. In spring, high primary production from sea ice algae and phytoplankton blooms led to spikes in pH ($pH > 8$) and aragonite oversaturation. In late fall, strong wind-driven mixing events that delivered low-CO_2 surface water to the shelf also led to events with elevated pH and Ω_{arag}. Given the recent observations of high rates of ocean acidification and a sudden and dramatic shift of the physical, biogeochemical, and ecosystem conditions in the Chukchi Sea, it is possible that the observed extreme conditions at the Chukchi Ecosystem Observatory are deviating from the carbonate conditions to which many species are adapted.

1 Introduction

The quickly changing Arctic Ocean has climatic, societal, and geopolitical implications for the peoples of the Arctic and beyond (Huntington et al., 2022). Arctic Indigenous Peoples are at the forefront of this change and their food security, food sovereignty, culture, and ways of life depend on healthy Arctic marine ecosystems (ICC, 2015). The Arctic is warming at a rate that is up to 4 times that of the rest of the globe (Serreze and Barry, 2011; Serreze and Francis, 2006; Rantanen et al., 2022). This phenomenon, called Arctic amplification, is observed in air and sea temperatures, has accelerated in recent years, and is expected to continue in the future (Rantanen et al., 2022; Shu et al., 2022). Warming exerts a toll on sea ice extent, ice thickness, and the duration of seasonal sea ice cover: ice is forming later in fall and retreating earlier in spring, thereby increasing the length of the open-water period (Stroeve et al., 2011; Serreze et al., 2016; Wood et al., 2015; Stroeve et al., 2014). The lowest Arctic-wide minimum sea ice extents were recorded during the last 16 years of the 44-year-long satellite time series (DiGirolamo et al., 2022).

At the same time, the Arctic Ocean is vulnerable to ocean acidification. Although oceanic uptake of anthropogenic carbon dioxide (CO_2) increases oceanic CO_2 and decreases pH and calcium carbonate ($CaCO_3$) saturation states of calcite (Ω_{calc}) and aragonite (Ω_{arag}) globally, climate-induced changes to riverine input, temperature, sea ice, and circulation are accelerating the rate of ocean acidification in the Arctic Ocean like nowhere else in the world (Woosley and Millero, 2020; Qi et al., 2022a; Yamamoto-Kawai et al., 2009; Orr et al., 2022; Semiletov et al., 2016; Qi et al., 2017). Recent observational studies propose that freshening of the Arctic Ocean due to increased riverine input may play an even greater role in acidifying the Arctic Ocean than the uptake of anthropogenic CO_2 (Woosley and Millero, 2020; Semiletov et al., 2016). In addition, the cold Arctic waters have naturally low concentrations of carbonate ions (CO_3^{2-}) and are therefore closer to aragonite undersaturation ($\Omega_{arag} < 1$) than more temperate waters (Orr, 2011; Sarmiento and Gruber, 2006), which leads to the chemical dissolution of free aragonitic $CaCO_3$ structures (Bednaršek et al., 2021). Because of the naturally low concentrations of CO_3^{2-}, such high-latitude waters have a lower capacity to take up anthropogenic CO_2 and buffer these changes (Orr, 2011). As a result, concentrations of hydrogen ions (H^+) increase and pH decreases faster in the Arctic than in the tropics, for example.

In the Pacific Arctic, the Chukchi shelf waters have warmed by 0.45 °C per decade since 1990, triple the rate since the beginning of the data record in 1922 (Danielson et al., 2020). Direct observations of the inorganic carbon dynamics of the Chukchi Sea are mostly limited to June through November because of the region's remoteness and accessibility during sea-ice-covered months. Summertime profiles across the Chukchi Sea show steep vertical gradients in inorganic carbon chemistry (Bates, 2015; Bates et al., 2009; Pipko et al., 2002; Mathis and Questel, 2013). Surface waters have a low partial pressure of carbon dioxide (pCO_2) as a result of high primary production after sea ice retreat, leading to aragonite supersaturated conditions, with $\Omega_{arag} < 2$ (Bates, 2015; Bates et al., 2009). In areas with sea ice melt or riverine freshwater influence, Ω_{arag} tends to be lower and at times undersaturated (Bates et al., 2009; Yamamoto-Kawai et al., 2009). At the same time, pCO_2 values near the seafloor are around 1000 µatm as a result of organic-matter remineralization, leading to summertime aragonite undersaturation (Mathis and Questel, 2013; Pipko et al., 2002; Bates, 2015). Between September and November, continuous measurements from within a few meters of the surface suggest a mosaic of pCO_2 levels between $\sim$ 200 to 600 µatm, likely due to patchy wind-induced mixing entraining high-CO_2 waters from depth into the surface mixed layer (Hauri et al., 2013). Yamamoto-Kawai et al. (2016) used mooring observations of S, T, and apparent oxygen utilization to estimate dissolved inorganic carbon (DIC), total alkalinity (TA), and Ω_{arag} in bottom waters at their mooring site in the Hope Valley in the southwestern Chukchi Sea to give first insights into year-round variability of the inorganic carbon system. They found slightly less intense aragonite undersaturation in spring and winter compared to summer, with a net undersaturation duration of 7.5–8.5 months per year.

The Chukchi Ecosystem Observatory (CEO) is situated in a benthic hotspot (Fig. 1) where high primary production supports rich and interconnected benthic and pelagic food webs (Grebmeier et al., 2015; Moore and Stabeno, 2015). The benthos is dominated by calcifying bivalves, polychaetes, amphipods, sipunculids, echinoderms, and crustaceans (Grebmeier et al., 2015; Blanchard et al., 2013). Benthic foraging bearded seals (*Erignathus barbatus*), walrus (*Odobenus rosmarus divergens*), gray whale (*Eschrichtius robustus*), and seabirds feed on these calcifiers during the open-water season (Kuletz et al., 2015; Jay et al., 2012; Moore et al., 2022). The CEO site, located on the southern flank of Hanna Shoal, is a region of reduced stratification (relative to other sides of the shoal) that likely alternately feels the effects of differing flow regimes located to the west and to the east (Fang et al., 2020). Consequently, the site exhibits relatively weaker currents (Tian et al., 2021) and so is conducive to the deposition of sinking organic matter that in turn feeds the local benthos (Grebmeier et al., 2015). Prolonged open-water seasons during periods of high solar irradiance, in combination with an influx of new nutrients and wind mixing, are likely enhancing primary and secondary production as well as the advection of zooplankton (Lewis et al., 2020; Arrigo and van Dijken, 2015; Wood et al., 2015). These physical processes in turn fuel keystone consumers such as Arctic cod (*Boreogadus saida*) and upper trophic-level ringed seals (*Phoca hispida*), beluga (*Delphinapterus leucas*) and bowhead whales (*Balaena mysticetus*), and predatory polar bears (*Ursus arctos*) and Indigenous People who rely on the marine ecosystem for traditional and customary harvesting (Huntington et al., 2020).

Perturbation of the seawater carbonate system associated with ocean acidification and climate change can have significant physiological and ecological consequences for marine species and ecosystems (Doney et al., 2020). All parameters of the carbonate system (pH, pCO_2, Ω_{arag}, concentrations of HCO_3^-, CO_3^{2-}, etc.) have the potential to affect the physiology of marine organisms while a change in the saturation state (Ω) can lead to the dissolution of unprotected or "free" $CaCO_3$ structures. Recent work has highlighted the importance of local adaptation to the present environmental variability as a key factor driving species sensitivity to ocean acidification (Vargas et al., 2017, 2022). As carbonate chemistry conditions vary enormously between regions, marine organisms are naturally exposed to different selective pressures and can evolve different strategies to cope with low pH or Ω or high pCO_2. For example, the deep-sea mussel *Bathymodiolus brevior* living around vents at 1600 m depths is capable of precipitating calcium carbonate at pH ranging between

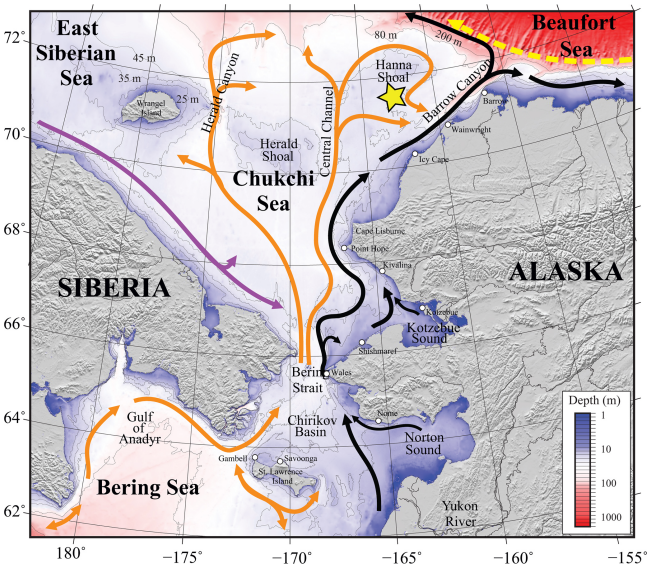

Figure 1. Map of the study area. Bathymetry of the Chukchi, northern Bering, East Siberian, and eastern Beaufort seas is shown in color. The Chukchi Ecosystem Observatory (CEO) location near Hanna Shoal is marked with a yellow star. General circulation patterns are shown with arrows: black – Alaskan Coastal Water and Alaskan Coastal Current, dividing into the Shelf-break Jet (right) and Chukchi Slope Current (left, Corlett and Pickart, 2017); orange – Anadyr, Bering, and Chukchi Seawater; purple – Siberian Coastal Current; yellow – Beaufort Gyre boundary current. Figure is from Hauri et al. (2018).

5.36 and 7.30 and highly undersaturated waters (Tunnicliffe et al., 2009). The response to changes in the carbonate chemistry is also modulated by other environmental drivers such as temperature or food availability (e.g., Thomsen et al., 2013; Breitberg et al., 2015). Consequently, no absolute or single threshold is expected for ocean acidification (e.g., Bednaršek et al., 2021) and a pre-requisite to assessing the impact on any biota is the monitoring at a short temporal scale to characterize the present environmental niche. When it comes to future impacts, the more intense and faster the changes associated with ocean acidification, the more adverse associated biological impacts are expected (Vargas et al., 2017, 2022). As a result, it is anticipated that Arctic marine waters that are experiencing widespread and rapid ocean acidification will potentially undergo severe negative ecosystem impacts (AMAP, 2018).

Here, we present satellite sea ice coverage data and 4 years of nearly continuous salinity, temperature, and pCO_2 data, accompanied by pH, nitrate (NO_3), dissolved oxygen (O_2), and chlorophyll fluorescence data for some of the time (Table 1, Figs. 2 and 3). We develop an empirical equation for estimating pH from moored pCO_2, temperature, and salinity and evaluate it using discrete samples collected across the Chukchi Sea, Bering Sea, and Beaufort Sea. Our time series allow us to assess the seasonal and interannual variability and controls of the inorganic carbon system in the Chukchi Sea between 2016 and 2020 and characterize the chemical conditions experienced by organisms. We discuss our observations in terms of progressing acidification and implications to organisms in the Chukchi Sea region.

2 Materials and methods

2.1 The Chukchi Ecosystem Observatory (CEO)

The Chukchi Sea is a shallow shelf sea with maximum depths < 50 m. It is largely a unidirectional inflow shelf system with Pacific origin water entering the Chukchi Sea through the Bering Strait and advecting north into the Arctic Ocean (Carmack and Wassmann, 2006). The CEO (71°36′ N, 161°30′ W; Fig. 1, reprinted from Hauri et al., 2018) is located along the pathway of waters flowing through Bering Strait (Fang et al., 2020) and thence from the west of Hanna Shoal toward Barrow Canyon to the south, although the wind can also drive waters from the east over the observatory site (Fang et al., 2020). From both shipboard and moored acoustic Doppler current profiler records, the south side of Hanna Shoal mean flow is characterized by a weak southward-directed current (Tian et al., 2021).

The observatory consists of oceanographic moorings that sample year-round, equipped with a variety of sensors that measure sea ice cover and thickness (Sandy et al., 2022), light, currents, waves, salinity, temperature, concentrations of dissolved oxygen, nitrate, and particulate matter, pH, pCO_2, chlorophyll fluorescence, zooplankton abundance and vertical migration (Lalande et al., 2021, 2020), the presence of Arctic cod and zooplankton (Gonzalez et al., 2021), and the vocalizations of marine mammals. During some years, the observatory included a third mooring, an experimental "freeze-up detection mooring", which transmitted real-time data of conductivity and temperature throughout the water column until sea ice formation. The primary moorings stretch from the seafloor at 46 m to about 33 m depth, designed to avoid collisions with ice keels. Pressure sensors at the top of the moorings show less than ± 1 m of excursion of the moored sensor package from its deployment mean depth in any given year, indicating that mooring blow-over or diving is not the cause of any observed large variability. Description of the CEO and lists of sensors deployed at the site can be found in Danielson et al. (2017) and Hauri et al. (2018). For this study we focus on the inorganic carbon system and its controlling mechanisms.

2.2 pCO_2

We used a CONTROS HydroC CO_2 sensor (4H-Jena Engineering GmbH, Kiel, Germany) to measure pCO_2. The CO_2 sensor was outfitted with a pump (SBE 5M, Sea-Bird Scientific) that flushes ambient seawater against a thin semi-permeable membrane, which serves as an equilibrator

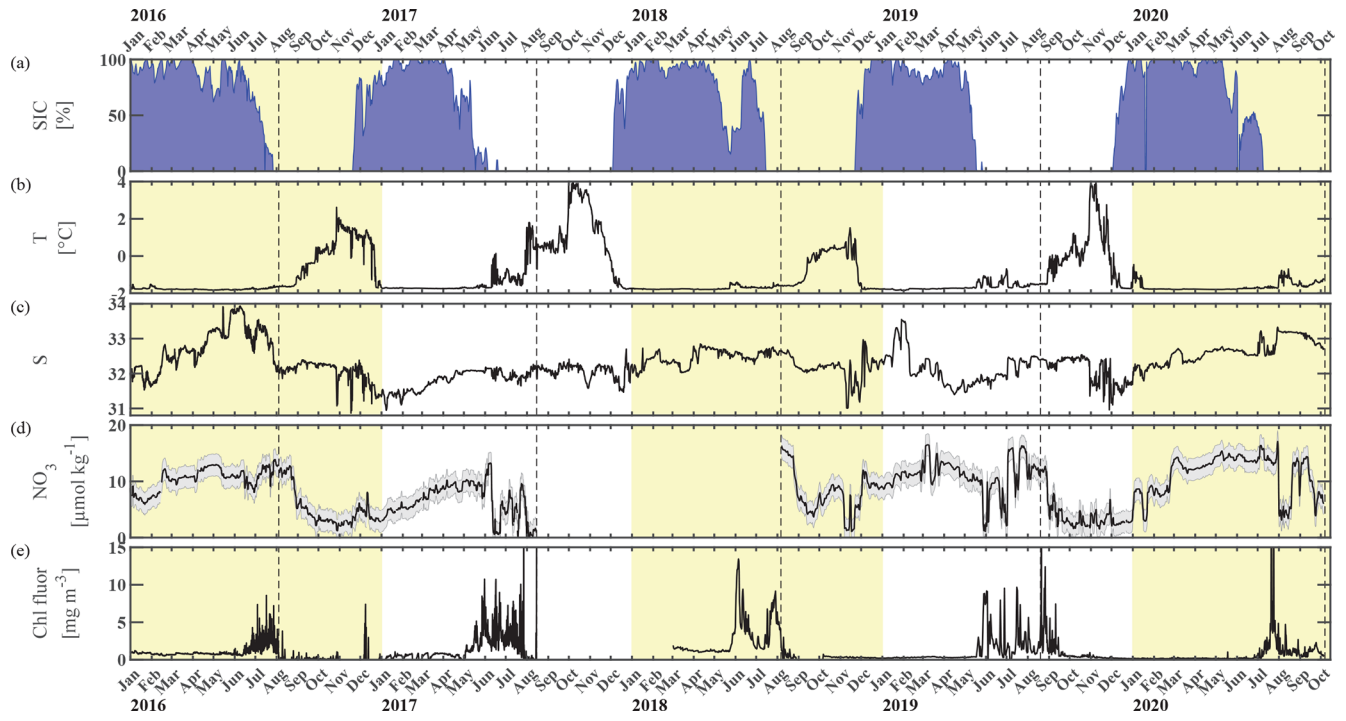

Figure 2. Chukchi Ecosystem Observatory time series from 2016 through 2020. **(a)** Sea ice concentration (blue shading to highlight coverage, %; DiGirolamo et al., 2022), **(b)** temperature (°C), **(c)** salinity, **(d)** NO_3 with uncertainty envelope (µmol kg^{-1}), and **(e)** chlorophyll fluorescence (mg m^{-3}). Years are indicated by alternating yellow and white background shading. The vertical dashed black lines indicate the mooring turnaround timing.

Table 1. Chukchi Ecosystem Observatory location and instrument sampling frequency. Sensor type and parameter measured (italicized) shown in top row. Values in parentheses indicate the number of measurements averaged over the measurement interval window.

Deployment	Latitude	Longitude	SUNA *NO_3*	HydroC CO_2 *pCO_2*	SBE 16 *CTD+*	SBE 37 *CTD*	SeaFET *pH*	SBE 63 *O_2*
2016–2017	71°35′58.5600″ N	161°31′06.2400″ W	1 h	12 h (300/5 min)*	1 h	–	–	–
2017–2018	71°35′58.9200″ N	161°31′08.0400″ W	1 h	12 h (5/5 min)	2 h	2 h	2 h (30/5 min)	2 h
2018–2019	71°35′59.6400″ N	161°31′41.1600″ W	1 h	24 h (5/5 min)	1 h	2 h*	–	2 h*
2019–2020	71°35′58.9200″ N	161°31′39.0000″ W	1 h	12 h (5/5 min)	2 h	–	–	–

* Indicates the sensor did not return data over the whole year due to battery failure. CTD+ indicates ancillary data was available with the SBE 16 file (e.g., chlorophyll fluorescence).

for dissolved CO_2 between the ambient seawater and the headspace of the sensor. Technical details about the sensor and its performance are described in Fietzek et al. (2014), who estimated sensor accuracy to be better than 1 % with post-processing.

A HydroC CO_2 sensor has been deployed at the CEO site since 2016. In all deployments, except in 2016, HydroC CO_2 sensors were post-calibrated. The lack of post-calibration in 2016 is not expected to negatively affect data quality because a battery failure resulted in data returns only over the first 3 months (August through November). Following a zero interval where the gas was pumped through a soda lime cartridge to create a zero-signal reference with respect to CO_2 and a subsequent flush interval to allow CO_2 concentrations to return to ambient conditions, measurements were taken in a burst fashion every 12 or 24 h depending on the deployment year (Table 1). Average pCO_2 values are reported as the mean of the measuring interval (Table 1) with standard uncertainty (Eq. 1) defined following best practices (Orr et al., 2018) and where the random component is the standard deviation of the mean and the systematic components include sensor accuracy and estimated error of the regression during calibration.

$$u = \sqrt{u^2_{\text{systematic}} + u^2_{\text{random}}} \quad (1)$$

More than 96 % of the time, the relative uncertainty of the pCO_2 data met the weather data quality goal, defined as 2.5 % by the Global Ocean Acidification Observing Network (GOA-ON; Newton et al., 2015).

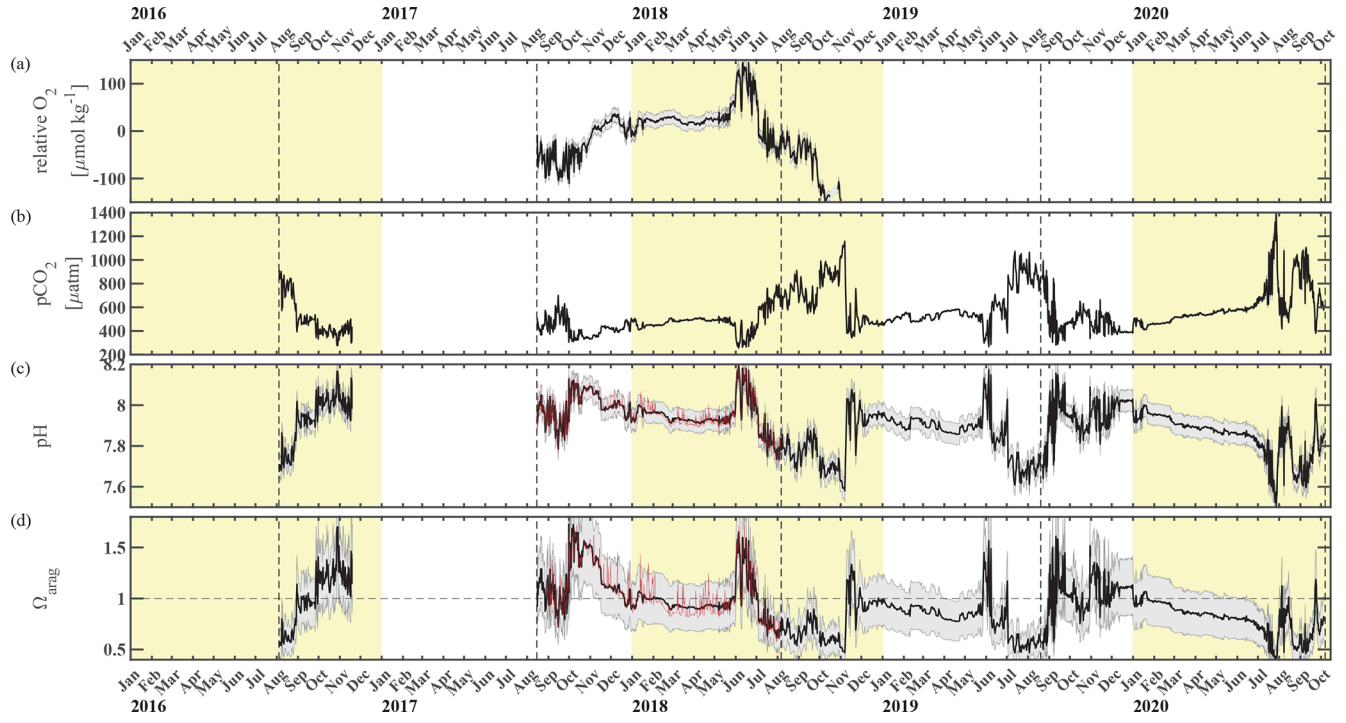

Figure 3. Chukchi Ecosystem Observatory time series from 2016 through 2020, part 2. **(a)** Relative dissolved oxygen with uncertainty envelope (relative to the mean; µmol kg^{-1}), **(b)** pCO_2 with uncertainty envelope (µatm; Hauri and Irving, 2023a), **(c)** pH with uncertainty envelope (pH^{est} in black, pH_{SeaFET} in red; Hauri and Irving 2023b), and **(d)** aragonite saturation state with uncertainty envelope ($\Omega_{arag}(pCO_2, pH^{est})$ in black; $\Omega_{arag}(pCO_2, pH_{SeaFET})$ in red). Years are indicated by alternating yellow and white backgrounds. The vertical dashed black lines indicate the mooring turnaround timing.

HydroC CO_2 data were processed using Jupyter Notebook scripts developed by 4H-Jena Engineering GmbH using pre- and post-calibration coefficients interpolated with any change in the zero-signal reference over the deployment (Fietzek et al., 2014). Further processing using in-house MATLAB scripts included removal of outliers, calculation of the average pCO_2, and calculation of uncertainty estimates for each measuring interval.

2.3 pH

A SeapHOx sensor (Satlantic SeaFET™ V1 pH sensor integrated with Sea-Bird Scientific SBE 37-SMP-ODO) was used to concurrently measure pH, salinity, temperature, pressure, and oxygen (Martz et al., 2010). A SeapHOx was deployed at CEO in 2016, 2017, and 2018. No SeapHOx was deployed in 2019 or 2020 due to supply chain delays and communication issues at sea. Unfortunately, measured pH (pH_{SeaFET}) from the 2016 and 2018 SeapHOx deployments were unusable due to high levels of noise in both the internal and external electrodes. In short, we only have usable pH data between August 2017 and August 2018.

pH_{SeaFET} data were excluded during a 14 d conditioning period following deployment and were processed with post-calibration corrected temperature and salinity from the SBE 37 following Bresnahan et al. (2014) using voltage from the external electrode (V_{ext}), and $pH_{V_{ext}}$ (pH calculated from the external electrode of the SeaFET) from an extended period of low variability (18 February 2018). Despite the availability of discrete data from one calibration cast (Cross et al., 2020b; Table 2), $pH_{V_{ext}}$ was used as the single calibration point (Bresnahan et al., 2014) for a variety of reasons: (1) there is high variability of pH_{SeaFET} (0.0581 pH units) straddling a 12 h window around the discrete sample collection time, (2) high temporal and spatial variability is often seen in the Chukchi Sea, and (3) the discrete pH sample was within the published SeaFET accuracy of 0.05 (Table 2, Fig. S1 in the Supplement). pH_{SeaFET} values are reported as the mean of the measuring interval (Table 1), and the standard uncertainty is calculated with Eq. (1) with the standard deviation of the average (random) and the SeaFET accuracy (systematic). Data handling and processing were done using in-house MATLAB scripts. pH is reported in total scale and at in situ temperature and depth for the entirety of this paper.

Table 2. Evaluation of pH_{SeaFET} and pH^{est} using reference pH from nearby discrete samples (pH^{disc}_{calc}). Uncertainty, u_c, is the propagated combined standard uncertainty from errors.m (Orr et al., 2018). pH_{SeaFET} and pH^{est} were interpolated to the discrete timestamp. See Fig. S1 for visualization of reference values.

Date	Cruise	Cast no.	Distance (km)	$pH^{disc}_{calc} \pm u_c$	Anomaly ($pH^{est} - pH^{disc}_{calc}$)	Anomaly ($pH_{SeaFET} - pH^{disc}_{calc}$)	Source
10 Sep 2017	HLY1702	127	0.52	8.0123 ± 0.0166	-0.0450*	-0.0354	Cross et al. (2020a)
11 Aug 2019	HLY1901	39	3.75	7.6423 ± 0.012	0.0079*	–	Cross et al. (2021)
19 Aug 2019	OS1901	33	0.27	7.7367 ± 0.0145	-0.0200	–	Claudine Hauri (unpublished data)

* Indicates pH^{disc}_{calc} was interpolated to mooring depth.

2.4 Nitrate

NO_3 measurements were from a Submersible Ultraviolet Nitrate Analyzer (SUNA) V2 by Sea-Bird Scientific. The SUNA is an in situ ultraviolet spectrophotometer designed to measure the concentration of nitrate ions in water. SUNA V2 data were processed using a publicly available toolbox (Hennon et al., 2022; Irving, 2021) with QA/QC steps that included thermal and salinity corrections (Sakamoto et al., 2009), assessment of spectra and outlier removal based on spectral counts (Mordy et al., 2020), and concentration adjustments (absolute offset and linear drift) based on pre-deployment and post-recovery reference measurements of zero-concentration (deionized, DI) water and a nitrate standard and, when available, nutrient samples taken from Niskin bottles near the mooring site (e.g., Daniel et al., 2020).

2.5 Conductivity–temperature–depth (CTD) and oxygen instruments

Two CTDs were deployed on the CEO mooring near the HydroC CO_2 depth. The main pumped Sea-Bird SeaCAT (SBE 16) has been deployed on the CEO mooring at around 33 m depth since 2014. A pumped SBE 43 oxygen sensor was deployed with the SBE 16 during the 2015–2016, 2017–2018, and 2019–2020 deployments, but only data returns from the 2017–2018 deployment are discussed briefly in this paper (Fig. S2).

The other pumped CTD was a Sea-Bird MicroCAT (SBE 37-SMP-ODO), which was integrated with an optical dissolved oxygen sensor (SBE 63; Fig. S2), and the SeaFET pH sensor within the SeapHOx instrument. The SeapHOx was deployed in fall 2016, 2017, and 2018. The SBE 37-SMP-ODO did not record any CTD or oxygen data during the 2016 deployment and only recorded CTD and oxygen data between August and 3 November 2018 due to battery failure.

Processing of these data included temperature and conductivity correction using pre- and post-calibration data following Seabird (2016) and oxygen correction using pre- and post-calibration data following Seabird (2023). Oxygen was converted from $mL\,L^{-1}$ to $\mu mol\,kg^{-1}$ following Bittig et al. (2018). Density and practical salinity were calculated using the TEOS-10 GSW Oceanographic Toolbox (McDougall and Baker, 2011).

Differences between the two oxygen sensors (SBE 43 and SBE 63) of approximately 145 to 265 $\mu mol\,kg^{-1}$ were observed over the 2017–2018 deployment, and both moored sensors had varying offsets compared to nearby casts (Fig. S2). Therefore, only relative oxygen values from the freshly calibrated SBE 63 are discussed in this paper.

The freeze-up detection mooring (Fig. 6) consisted of four Sea-Bird SBE 37 inductive modem CTD sensors that transmitted in real time hourly temperature, salinity, and pressure data via the surface float from four subsurface depths (8, 20, 30, and 40 m; Hauri et al., 2018).

2.6 Development of empirical relationship to estimate pH

Empirical relationships for estimating water column pH have been developed for regions spanning southern, tropical, temperate, and Arctic biomes, using a variety of commonly measured parameters (e.g., pH(S, T, NO_3, O_2, Si), Carter et al., 2018; pH(O_2, T, S), Li et al., 2016; pH(θ, O_2), Watanabe et al., 2020; pH(NO_3, T, S, P) and pH(O_2, T, S, P), Williams et al., 2016; pH(O_2, T), Alin et al., 2012; pH(O_2, T) and pH(NO_3, T), Juranek et al., 2009). Given the tight coupling between the concentration of H^+ and the concentration of the CO_2 solution, an empirical relationship for estimating surface pH from pCO_2 was developed by the National Academies of Sciences, Engineering and Medicine (2017, Appendix F). Licker et al. (2019) used this empirical relationship to calculate the global average surface ocean pH and found it represented the relationship for surface water temperatures spanning 5 to 45 °C. Here, we take a similar approach but extend it to water column pH in our cold region using temperature (T) and salinity (S) as additional proxy parameters (Eq. 2).

$$pH^{est} = \alpha_0 + \alpha_1 \log\,(pCO_2) + \alpha_2 T + \alpha_3 S, \quad (2)$$

where pH^{est} is the estimated value of water column pH, pCO_2 is from the HydroC, T and S are from the SBE 16, and all α ($\alpha_0 = 10.4660$, $\alpha_1 = -0.4088$, $\alpha_2 = 0.0013$, $\alpha_3 = -0.0001$) terms are model-estimated coefficients determined using MATLAB's multiple linear regression algorithm regress.m (Chatterjee and Hadi, 1986). After interpolating pH_{SeaFET} (Fig. 4, red dots) to the pCO_2 timestamp, the algorithm was trained over an arbitrarily chosen 180 d period (15 September 2017–14 March 2018, Fig. 4, dashed box). An uncertainty of 0.0525 for pH^{est} (Figs. 3 and S1, gray shading) was determined with Eq. (1), where the RMSE (the uncertainty in the estimation) over the entire pH_{SeaFET} time series is the random component and the published accuracy of the SeaFET is the systematic component (since the algorithm was trained with pH_{SeaFET}). The algorithm cross-validation and evaluation are discussed in Sect. 3.1. Unless explicitly defined otherwise, observations of pH refer to pH^{est} for the remainder of this paper.

2.7 Carbonate system calculations

Moored data were collected at different sample intervals (Table 1) and were linearly interpolated to the HydroC CO_2 timestamp to enable further calculations. TA, DIC, and Ω_{arag} (Figs. 11a, b and 3d) were calculated based on measured pCO_2, S, T, and pressure (P) and algorithm-based pH (pH^{est}). Due to a lack of data, nutrient concentrations (Si, PO_4, NH_4, H_2S) were assumed to be negligible in the CO2SYS calculations (e.g., DeGrandpre et al., 2019; Vergara-Jara et al., 2019; Islam et al., 2017). pH^{est} was used in lieu of pH_{SeaFET} to allow for calculations over the whole pCO_2 record and due to erroneously large variability of DIC and TA when pH_{SeaFET} was used as an input parameter (Raimondi et al., 2019; Cullison-Gray et al., 2011). The pH–pCO_2 input pair leads to large, calculated errors in DIC and TA (Raimondi et al., 2019; Cullison-Gray et al., 2011) due to strong covariance between the two parameters (both temperature and pressure dependent). Cullison-Gray et al. (2011) attributed unreasonably large short-term variability in calculated TA and DIC to temporal or spatial measurement mismatches between input pH and pCO_2 parameters and found that appropriate filtering alleviated noise spikes. By using pH^{est}, which by the nature of its definition is well correlated to pCO_2, we are eliminating some of these spurious noise spikes. We show Ω_{arag} calculated from pH_{SeaFET}-pCO_2 (Fig. 3d, red line) because it is less sensitive to calculated errors as it accounts for a small portion of the total CO_2 in seawater (Cullison-Gray et al., 2011).

All inorganic carbon parameters were calculated using CO2SYSv3 (Sharp et al., 2023; Lewis and Wallace, 1998) with dissociation constants for carbonic acid from Lueker et al. (2000), bisulfate from Dickson (1990), hydrofluoric acid from Perez and Fraga (1987), and the boron-to-chlorinity ratio from Lee et al. (2010). Sulpis et al. (2020) found that the carbonic-acid dissociation constants of Lueker et al. (2000) may underestimate pCO_2 in cold regions (below ~ 8 °C) and therefore overestimate pH and CO_3^{2-}. However, we choose to use Lueker et al. (2000) because they are recommended (Dickson et al., 2007; Woosley, 2021), continue to be the standard (Jiang et al., 2021; Lauvset et al., 2021), and are commonly used at high latitudes (Duke et al., 2021; Raimondi et al., 2019; Woosley et al., 2017). Furthermore, the difference between DIC calculated from pH^{est} and pCO_2 and discrete samples interpolated to moored instrument depth ranged from 266 to $-195\,\mu mol\,kg^{-1}$ using the K_1^* and K_2^* of Sulpis et al. (2020), compared to -38 to $-7\,\mu mol\,kg^{-1}$ using Lueker et al. (2000).

2.8 Sea ice concentration

Sea ice concentration at the observatory site was taken from the National Snow and Ice Data Center (NSIDC; DiGirolamo et al., 2022). Latitude and longitude coordinates were converted to NSIDC's EASE grid coordinate system (Brodzik and Knowles, 2002) and the 25 km gridded data were bilinearly interpolated to calculate sea ice concentration at the CEO site. Low sea ice is defined by < 15 % sea ice coverage per grid cell.

2.9 Estimation of model-based ocean acidification trend

Model results were obtained from historical simulations of five different global Earth system models: (1) GFDL-CM4 (Silvers et al., 2018), (2) GFDL-ESM4 (Horowitz et al., 2018), (3) IPSL-CM6A-LR-INCA (Boucher et al., 2020), (4) CNRM-ESM2-1 (Seferian, 2019), and (5) the Max Plank Earth System Model 1.2 (MPI-ESM1-2-LR; Wieners et al., 2019) that are part of the Coupled Model Intercomparison Project Phase 6 (CMIP6). Each simulation was used to calculate the annual trend in Ω_{arag} and pH at the closest depth and grid cell to the CEO mooring.

3 Results

In the following, we will evaluate the pH algorithm (Sect. 3.1), analyze the large variability patterns (Sect. 3.2 and 3.3), and then take a closer look at the data from 2020 since the seasonal cycle was different in 2020 compared to previous years (Sect. 3.4).

3.1 pH algorithm

The algorithm estimated pH data from the CEO site reasonably well and within the weather uncertainty goal as defined by Newton et al. (2015) most of the time. As a first step, pH^{est} consistency was assessed through cross-validation (Fig. 5) using the test dataset (outside the training period; $r^2 = 0.9666$, RMSE = 0.166) and across the whole time series ($r^2 = 0.9598$, RMSE = 0.0161, $p < 0.0001$; Fig. 5). Ob-

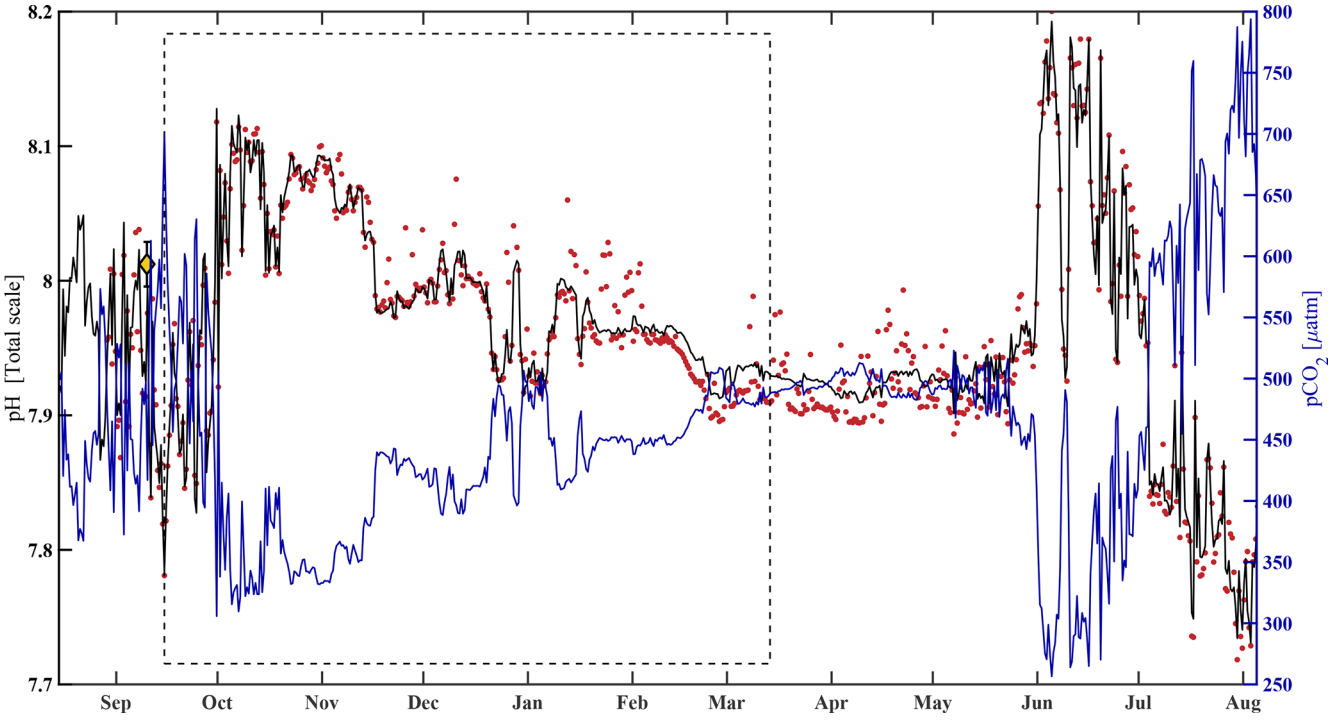

Figure 4. HydroC pCO_2 and pH highlighting mirrored trend from mid-August 2017 to beginning of August 2018. Measured pH (pH_{SeaFET}, red dots) is interpolated onto the HydroC pCO_2 timestamp (blue), and pH^{est} is shown as the solid black line. The dashed box shows the period over which pH^{est} was trained. The yellow diamond with error bars shows reference $pH^{disc}_{calc} \pm u_c$ (Table 2; Cross et al., 2020a; Orr et al., 2018).

served high-frequency spikes in pH_{SeaFET} (Fig. 4, red dots; Fig. 5d, red line) were not captured by the HydroC pCO_2 sensor (sampling frequency of 12 h) and, as a result, are not reproduced in the pH^{est} time series. Throughout the pH_{SeaFET} time series, pH^{est} overestimates pH_{SeaFET} by a mean of 0.0008 and median of 0.0039. Since pH^{est} generally overestimates pH_{SeaFET}, we assume that Ω_{arag} is also somewhat overestimated throughout this paper. Discrete water samples were used as reference values to evaluate the algorithm at the CEO site (Table 2) and were found to be within the pH^{est} uncertainty (Fig. S1).

An independent verification of our algorithm was done using discrete data collected from the Bering Sea to the Arctic Ocean on four research cruises in 2020, 2019, 2018, and 2017 (Fig. 6d; Monacci et al., 2022; Cross et al., 2021, 2020a, b), henceforth called the DBO dataset. Samples collected from deeper than 500 m below the surface or flagged as questionable or bad were excluded from this analysis. pH and pCO_2 were calculated from 1275 discrete samples analyzed for TA, DIC, silicate, phosphate, and ammonium (except when silicate, phosphate, and ammonium were assumed to be negligible for the 327 samples from cruise SKQ202014S; Monacci et al., 2022) using CO2SYSv3 (Sharp et al., 2023; Sect. 2.7 for details) and are referred to as pH^{disc}_{calc} and $pCO_2^{disc}_{calc}$, respectively. pH^{disc}_{est} was based on discrete water samples and calculated using Eq. (2) and was fit to pH^{disc}_{calc} using a linear regression ($r^2 = 0.9975$, RMSE = 0.0078, p value < 0.0001; Fig. 6a–c). Mean and median differences between pH^{disc}_{calc} and pH^{disc}_{est} were 0 and 0.0022, respectively, with the largest anomalies observed at lower salinities (Fig. 6c). Absolute differences between pH^{disc}_{est} and pH^{disc}_{cal} over the salinity range observed at the CEO site (30.87 to 33.93) fall within the weather data quality goal (Newton et al., 2015) 98.7 % of the time with maximum absolute differences < 0.03. The uncertainty of 0.0154 for pH^{disc}_{est} was determined using Eq. (1), where the mean combined standard uncertainty (u_c) for pH^{disc}_{calc} (0.0133; Orr et al., 2018) was the systematic component, and the regression RMSE was the random component.

Empirical relationships for estimating water column pH that rely on dissolved oxygen often ignore surface waters to limit biases due to decoupling the stoichiometry of the $O_2 : CO_2$ relationship due to air–sea gas exchange (e.g., Juranek et al., 2011; Alin et al., 2012; Li et al., 2016). We see evidence of this bias in our algorithm at low salinity (Fig. 6c) and low pCO_2 (not shown) when compared with the DBO dataset samples collected across the Arctic and from the surface to 500 m, with pH^{disc}_{est} overestimating pH^{disc}_{calc} by a maximum of 0.049. If depth is restricted to between 30 and 500 m when evaluating the algorithm with the DBO dataset, algorithm performance improves ($r^2 = 0.9990$, RMSE = 0.0055,

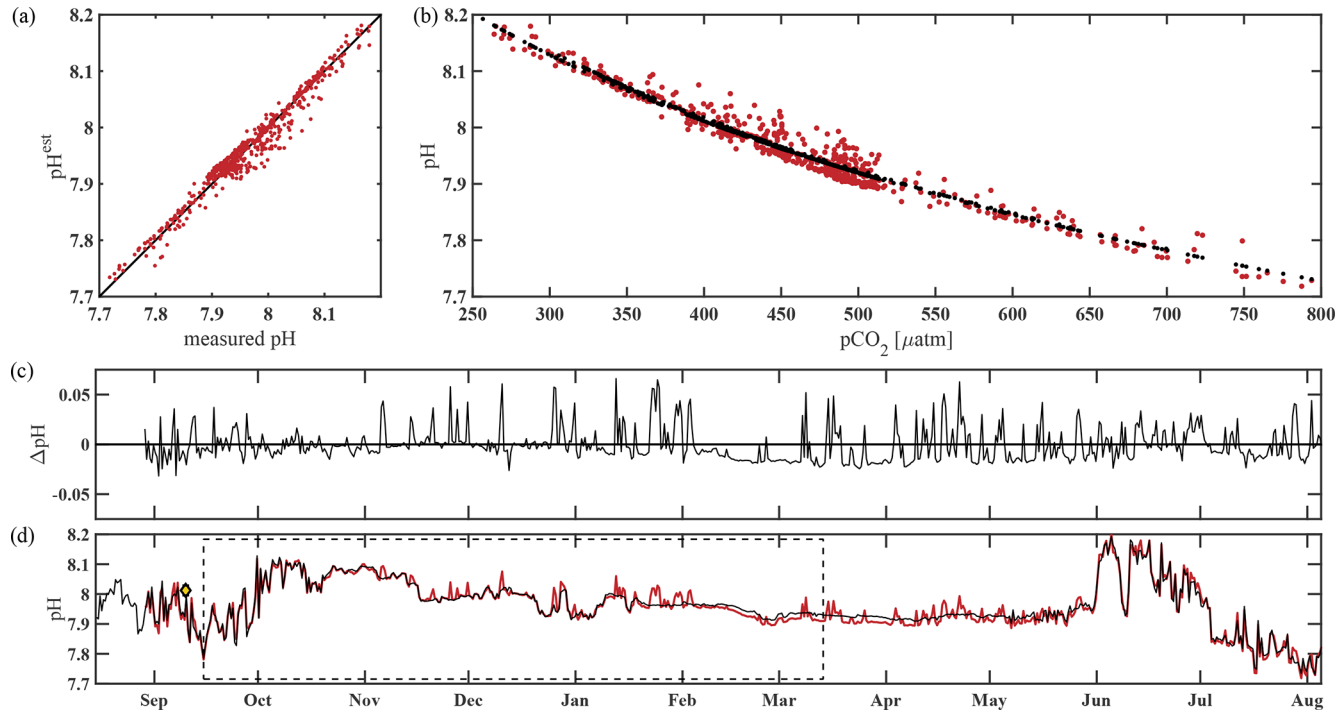

Figure 5. Performance of the pH algorithm. **(a)** pH_{SeaFET} vs. pH^{est} with black line highlighting 1 : 1 ratio, **(b)** pCO_2 vs. pH_{SeaFET} (red) and pCO_2 vs. pH^{est} (black), **(c)** residual pH ($pH_{SeaFET} - pH^{est}$), and **(d)** pH_{SeaFET} (red) and pH^{est} (black) vs. time, with dashed box highlighting the period over which pH^{est} was trained (15 September–14 March 2017) and the yellow diamond with error bars showing reference $pH^{disc}_{calc} \pm u_c$ (Table 2; Cross et al., 2020).

p value < 0.0001; not shown) and the maximum pH^{disc}_{est} overestimates pH^{disc}_{calc} by 0.022.

3.2 Relaxation events

The sub-surface waters at the CEO site comprise a high-pCO_2, low-pH, and low-Ω_{arag} environment, with mean values of $pCO_2^{mean} = 538 \pm 7$ µatm, $pH^{mean} = 7.91 \pm 0.05$, and $\Omega_{arag}^{mean} = 0.94 \pm 0.23$ across the full data record (Fig. 3b–d). In the following we will focus on spikes in high pH and Ω_{arag} and low pCO_2 that occur in spring (May–June) and fall (September–December); we define these spikes as relaxation events (see discussion for justification of term).

Spring. Springtime relaxation events at 33 m depth that exhibit relatively higher pH and Ω_{arag} and lower pCO_2 compared to the overall mean are likely consequences of photosynthetic activity during sea ice break-up (Figs. 2 and 3). In June of 2018 and 2019, near-bottom pH and Ω_{arag} spiked to > 8.17 and > 1.5, respectively, while pCO_2 dropped to $<$ 286 µatm. Ω_{arag} remained oversaturated and pH was greater than 8.0 for nearly all of June in 2018. In 2019, the relaxation event was less sustained, with only four short (2–6 d long) events of relatively higher pH and $\Omega_{arag} > 1$ in June. In both years, chlorophyll fluorescence spiked and either O_2 increased (in 2018) or NO_3 decreased (in 2019), which are signs of photosynthetic activity and primary production.

Fall. The relaxation events in fall were characterized by large and sudden drops in pCO_2, abrupt increases in pH and Ω_{arag}, and considerable interannual variability in their timing. Unlike the relaxation events observed in spring, we attribute these fall relaxation events to wind-induced physical mixing. To examine the controlling mechanisms causing these abrupt relaxation events in fall, we will start with using water column salinity and temperature data from a freeze-up detection buoy (Hauri et al., 2018) that was deployed in summer 2017 approximately 1 km away from the biogeochemical mooring. The freeze-up detection mooring provided temperature and salinity measurements every 7 m throughout the water column from the time of its deployment in mid-August until freeze-up. Data from the freeze-up detection mooring suggest that warmer and fresher water from the upper water column gets periodically entrained down to the location of the biogeochemical sensor package at 33 m depth, leading to enhanced variability of density in August and September (Fig. 7). Fluctuations of the pycnocline associated with the passage of internal waves could also elevate signal variances. During this time pCO_2 often decreased to or below atmospheric levels and pH sporadically reached values > 8. At the end of September, a strong mixing event (with coincident strong surface winds) homogenized the water column from the surface down to the location of the sensor package and caused a sudden temperature increase from 0.4 to 3.9 °C

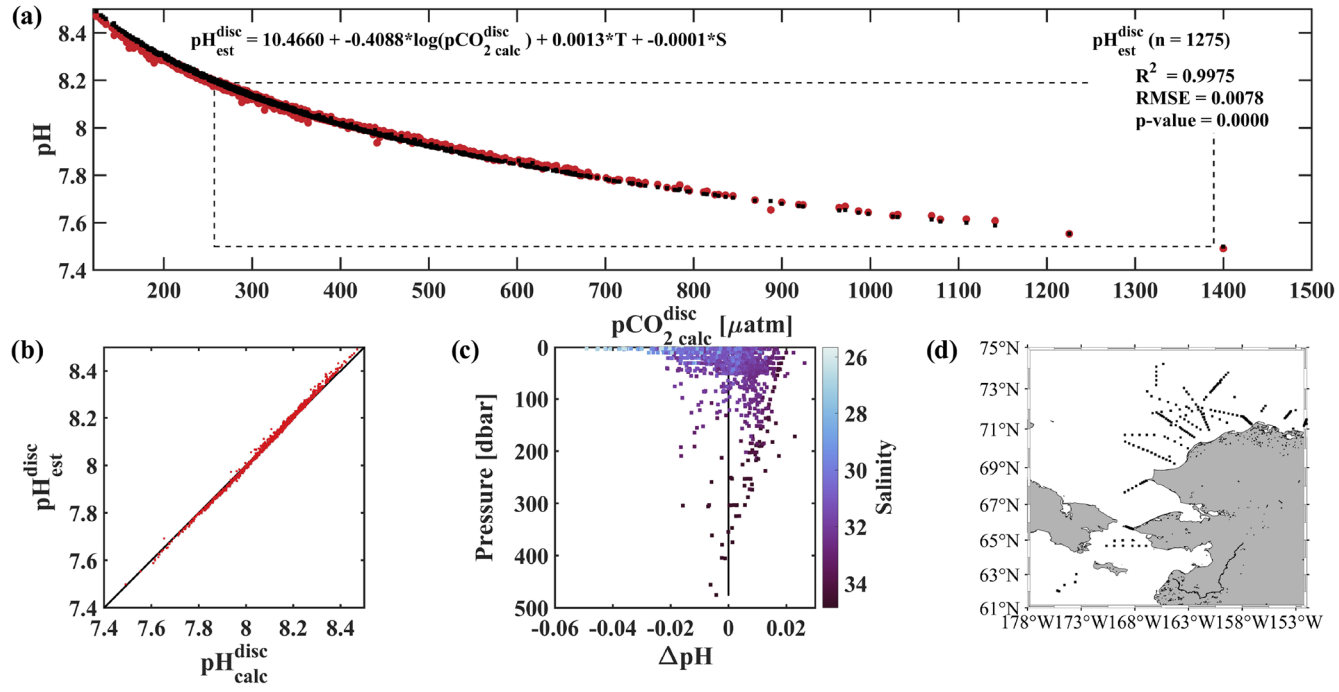

Figure 6. Evaluation of the pH algorithm. pH^{est} evaluation with pH^{disc}_{calc} from discrete samples collected during four cruises in the fall or early winter (August–November) of 2017–2020 and pH^{disc}_{est} from our linear regression model (Eq. 2). **(a)** $pCO_2{}^{disc}_{calc}$(TA, DIC) vs. pH (red pH^{disc}_{calc} and black pH^{disc}_{est}) with dashed black box showing the range of pH and pCO_2 observed at the CEO at 33 m depth, **(b)** pH^{disc}_{calc} vs. pH^{disc}_{est} with black 1 : 1 ratio, **(c)** residual pH ($pH^{disc}_{calc} - pH^{disc}_{est}$) vs. depth with color shading by salinity and black vertical line at 0, and **(d)** map showing the locations of the 1275 discrete water samples used for evaluation (Monacci et al., 2022; Cross et al., 2021, 2020a, b).

(Figs. 7c and 8a). At the same time, pCO_2 (Figs. 7b and 8) decreased from 590 to 308 µatm. This suggests that warm and low-CO_2 surface water mixed with CO_2-rich subsurface water and led to a sustained relaxation period that subsequently lasted until mid-November. Another mixing event further eroded the water column stratification and replaced subsurface water with colder and fresher water (ice melt) from the surface at the end of October. This second large mixing event did not lead to large changes in pCO_2, pH, and Ω_{arag}.

Salinity and temperature records from the biogeochemical mooring at 33 m depth also suggest fall season mixing events in all other years, when increases in temperature coincide with decreases in pCO_2 (Figs. 2b and c, 3a and 8). For example, two mixing events shaped the carbonate chemistry evolution in fall 2018. pCO_2 decreased from 915 µatm to around 565 µatm and Ω_{arag} increased to 0.9 as temperature increased and salinity decreased in early September (Figs. 2 and 8). pCO_2 then increased to 1160 µatm in late October, before decreasing to 385 µatm at the beginning of November, causing a spike in Ω_{arag} to 1.34. At the same time, salinity decreased by 1 unit, suggesting a strong mixing event. Throughout November 2018, pCO_2 oscillated between 344 and 757 µatm and salinity between 31.01 and 32.97, hinting at additional mixing.

Similarly, an early mixing event in 2019 decreased pCO_2 to 352 µatm at the beginning of September. Short-term variability in pCO_2 with maximum levels of up to 855 µatm and minimum values below 300 µatm, variable temperature and salinity, and sporadic aragonite oversaturation events point to mixing through mid-September. At the end of October, a large mixing event homogenized the water column, accompanied by a decline in salinity by > 1 unit, an increase in temperature to 4 °C, and a decrease in pCO_2 from 565 µatm to below 400 µatm. In a similar fashion to 2018, this fall mixing event was followed by a month-long period of large variability of pCO_2, salinity, pH, and Ω_{arag}, leading to short and sporadic aragonite oversaturation events in November and sustained oversaturation in December.

3.3 Sustained periods of low pH and Ω_{arag} and high pCO_2

Waters at 33 m depth at the CEO site were most acidified during the sea-ice-free periods until mixing events entrained surface waters to the sensor depth (Sect. 3.2). pH and Ω_{arag} started to gradually decrease from their maximum levels ($\Omega_{arag\_max} = 1.65$, $pH_{max} = 8.19$) at the beginning of June in 2018 to their annual low at the beginning of November ($\Omega_{arag\_min} = 0.47$, $pH_{min} = 7.58$; Fig. 3d and c). In November, the waters were also undersaturated with regards to cal-

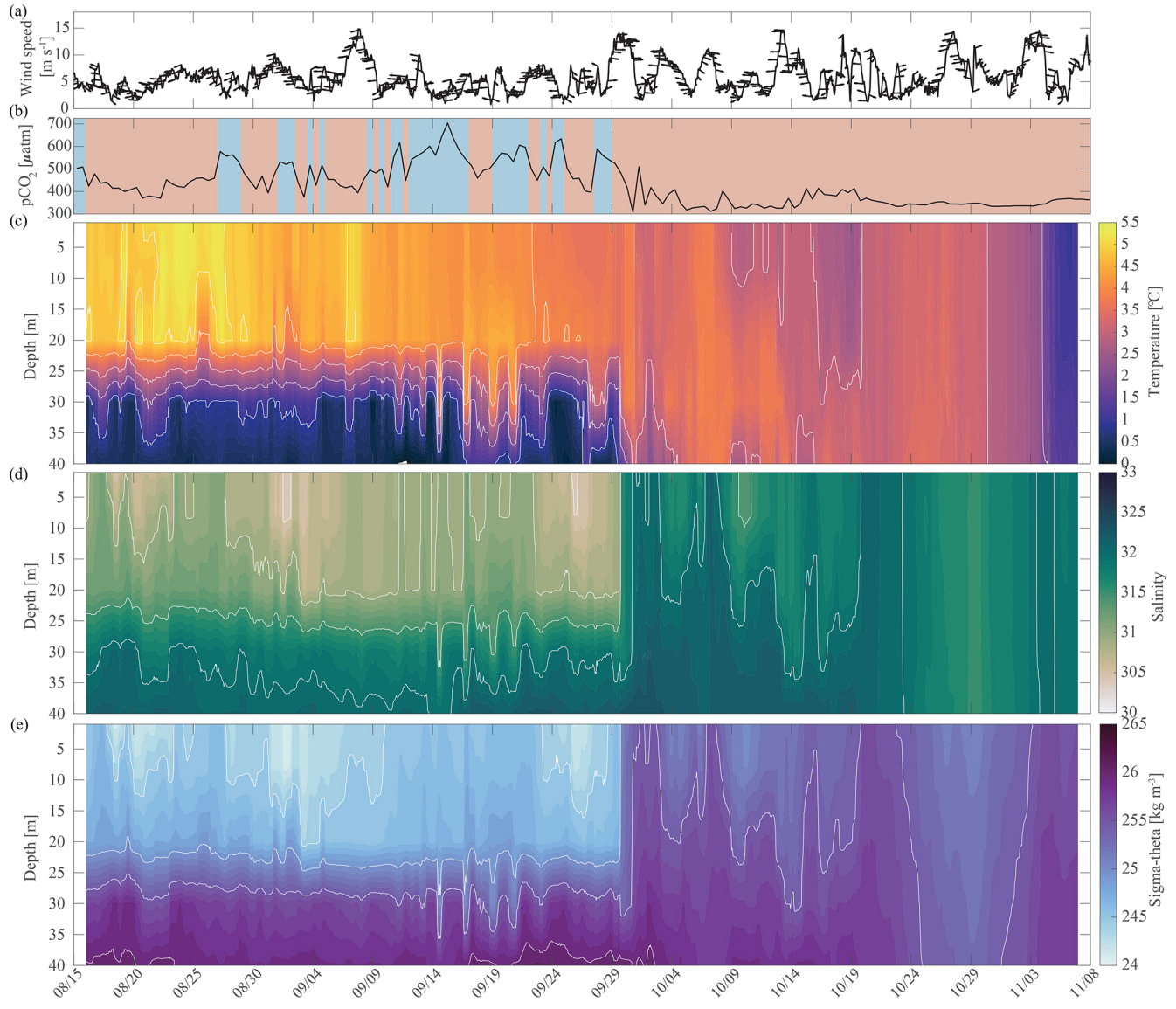

Figure 7. Water column structure from late summer 2017 to freeze-up. Profiles of **(a)** wind speed and direction (arrows pointing downwind) from the NOAA-operated Wiley Post–Will Rogers Memorial Airport, **(b)** pCO_2 (µatm) with blue background indicating the water was undersaturated regarding aragonite ($\Omega_{arag} < 1$) and red shading indicating aragonite oversaturation ($\Omega_{arag} >= 1$), **(c)** temperature (°C), **(d)** salinity, and **(e)** sigma-theta (kg m^{-3}). Temperature **(c)** and salinity **(d)** were measured at 8, 20, 30, and 40 m by the Chukchi Ecosystem Observatory freeze-up detection mooring deployed in fall 2017. Density was calculated with the TEOS-10 GSW Oceanographic Toolbox (McDougall and Baker, 2011).

cite (not shown), and pCO_2 peaked at 1159 µatm (Fig. 3b). Dissolved oxygen decreased by about 400 µmol kg^{-1} between July and October, when the sensor stopped working properly. The decrease in dissolved oxygen suggests remineralization of organic material. The decrease in pH, Ω_{arag}, and O_2 and the increase in pCO_2 was briefly interrupted by a strong mixing event in September, which entrained warmer, fresher, and CO_2-poorer water down to 33 m depth (Sect. 3.2, Fig. 8). The 2019 observations paint a similar picture of remineralization during the summer months, as the pCO_2 increase and pH and Ω_{arag} decreases were accompanied by an NO_3 increase (Fig. 2d and 3b–d).

pCO_2 steadily increased and pH and Ω_{arag} decreased during the sea-ice-covered periods (Fig. 8). pH was < 8 and Ω_{arag} remained undersaturated under the sea ice. At the same time, NO_3 slowly increased and O_2 decreased, which points to slow organic-matter remineralization (Fig. 9). Short-term variability in pCO_2, especially in January of all three observed years, was also reflected in salinity, O_2, and NO_3 (Fig. 9) and could be attributed to advection, as the CEO site

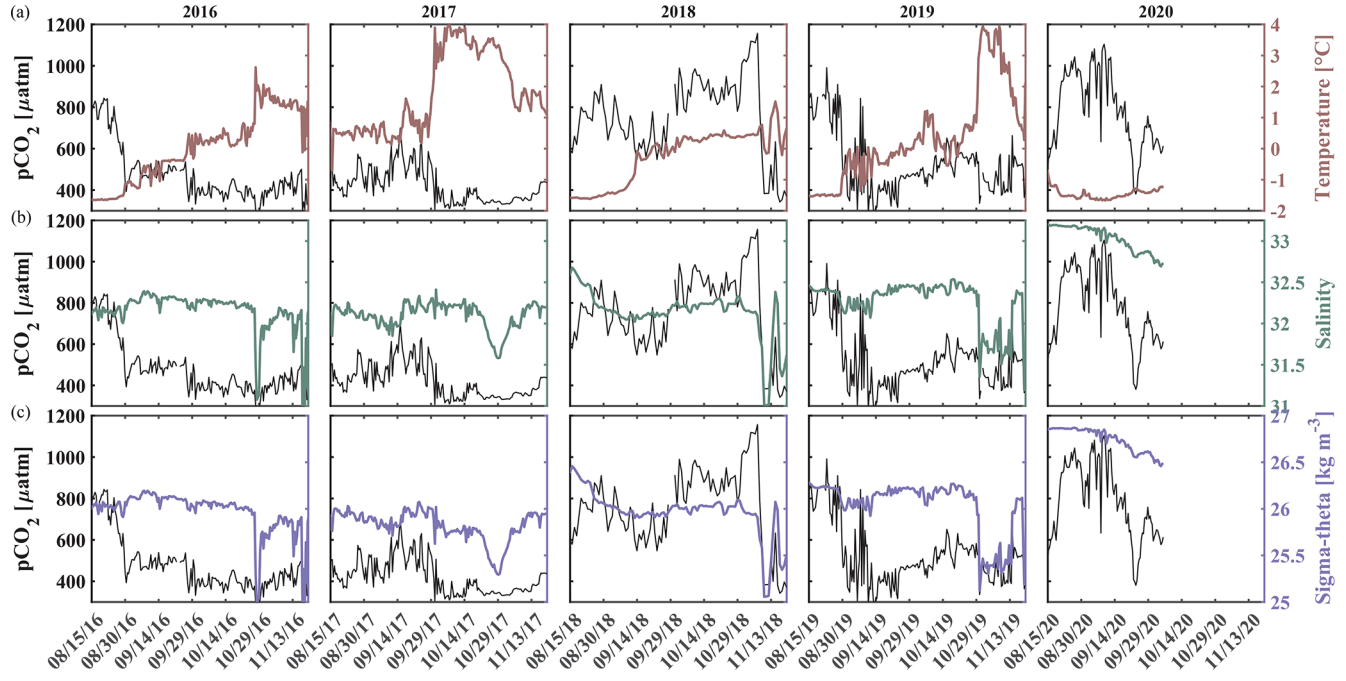

Figure 8. Impact of water column mixing on pCO_2. Time series of pCO_2 (black, left axis) and **(a)** temperature (maroon, right axis), **(b)** salinity (green, right axis), and **(c)** density (purple, right axis) for 15 August to 1 December in 2016–2020 measured at ∼ 33 m depth at the Chukchi Sea Ecosystem Observatory.

is adjacent to contrasting regimes of flow and hydrographic properties (Fang et al., 2020).

3.4 Spring and summer of 2020 were different

The seasonal cycle in 2020 strongly contrasted with the previous observed years. pCO_2 gradually increased by roughly 200 µatm throughout the sea-ice-covered months to 650 µatm when sea ice started to retreat at the beginning of July. By the end of July, pCO_2 doubled and increased to 1389 µatm, which is the highest pCO_2 level recorded in this time series. The peak of pCO_2 was accompanied by an increase in salinity of 0.5, while temperature did not change, suggesting the influence of advection. At the beginning of August, pCO_2 dropped to 536 µatm and then oscillated around 600 µatm through much of August before returning to around 900 µatm for the next month. Similarly, pH decreased to 7.5 at the end of July and then oscillated around 7.85, while Ω_{arag} dropped to 0.37 and oscillated around 0.85. The steep drop and oscillation of pCO_2 was reflected in NO_3, suggesting that primary production and remineralization played a role. When pCO_2 and NO_3 decreased at the beginning of August, temperature simultaneously increased by 0.7 °C and salinity decreased by 0.12, suggesting that entrainment of shallower water masses may have played a role too. Comprehensive analyses of the factors that resulted in the 2020 differing conditions are beyond the scope of this paper but deserve attention in a future effort.

4 Discussion

CEO data provide new insights into the synoptic, seasonal, and interannual variability of the inorganic carbon system at a time when ocean acidification and climate change have already started to transform this area. The observations suggest that the CEO site is a high-CO_2 and low-pH and low-Ω_{arag} environment most of the time, except during sea ice breakup when the effects of photosynthetic activity remove CO_2 from the system and later in fall, when strong storm events entrain low-pCO_2 surface waters to the seafloor. Lowest pH and $CaCO_3$ saturation states and highest pCO_2 occur in summer through late fall when organic-matter remineralization dominates the carbonate system balance. During this time, Ω_{arag} can fall below 0.5 and even Ω_{calc} becomes sporadically undersaturated ($\Omega_{calc} < 1$).

4.1 pH algorithm

Deploying oceanographic equipment in remote Arctic locations is challenging. The data return from the SeapHOx sensors was disappointingly minimal, despite annual servicing and calibration by the manufacturer. Our new pH algorithm is therefore even more important as it fills pH data gaps in the CEO time series and can be applied with confidence from the Bering to the western Beaufort seas (Fig. 6). While another successful year of moored pH data return at the CEO site is needed to fully evaluate our algorithm throughout the year, comparison with single discrete water samples near the

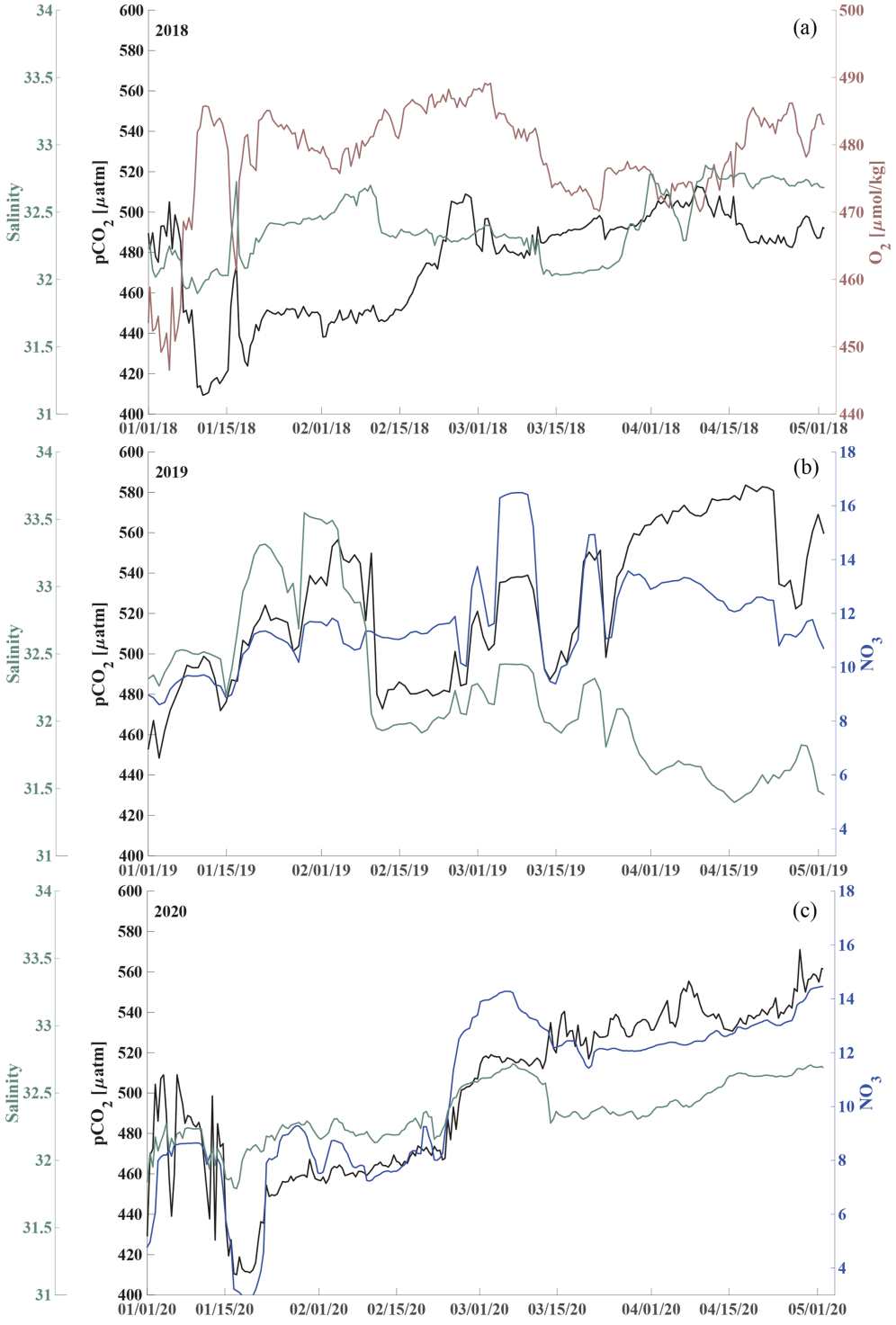

Figure 9. Respiration under the sea ice. Time series of pCO_2 (black), salinity (green, left axis), and oxygen (O_2, µmol kg^{-1}, maroon, panel **a**) and nitrate (NO_3, µmol kg^{-1}, blue, panels **b, c**) concentration (right axis during January through April for 2018, panels **a**, 2019 **b** and 2020 **c**).

CEO site and the DBO dataset (Sect. 3.1, Table 2, Figs. 6 and S1) suggest that our algorithm-derived pH meets the weather quality uncertainty goal of ±0.02 (Newton et al., 2015) much of the time.

The combination of our new algorithm with recent progress in monitoring pCO_2 with seagliders (Hayes et al., 2022) will further increase our ability to study the inorganic carbon dynamics at times and locations when shipboard or mooring-based measurements may not be practical. Additional assessment is needed to determine to what degree the algorithm needs adjustments beyond the region evaluated in this work.

4.2 Uncertainty

Inherent spatial and temporal variability of the inorganic carbon parameters in the Chukchi Sea make the use of discrete water samples for evaluating sensor-based measurements difficult. Historic continuous surface measurements from the area suggest that surface pCO_2 can be as low as < 250 µatm in early fall (Hauri et al., 2013), at a time of year when subsurface pCO_2 reaches its maximum of > 800 µatm at the CEO site. This suggests a steep pCO_2 gradient of $> 17\,\mu\text{atm}\,\text{m}^{-1}$. High-resolution pH data from the 2017/2018 deployment suggests high temporal variability as well, further complicating the collection of discrete water samples to adequately evaluate the sensors. The HydroC's zeroing function, in addition to our pre- and post-calibration routines that factor into the post-processing of the data, gives us confidence in the accuracy of the pCO_2 data and further confidence in pH derived from pCO_2.

The pH^{est} uncertainty of 0.0525 is likely a conservative estimate based on our validation of pH^{est} (Sect. 3.1, Table 2). Consequently, propagated uncertainties in the calculated parameters are high. As discussed in Sect. 2.7, the pH–pCO_2 input pair exacerbates these larger uncertainties. Mean TA(pH^{est}, pCO_2), DIC(pH^{est}, pCO_2), and Ω_{arag}(pH^{est}, pCO_2) $\pm u_c$ (Orr et al., 2018) are $2173 \pm 281\,\mu\text{mol}\,\text{kg}^{-1}$, $2111 \pm 263\,\mu\text{mol}\,\text{kg}^{-1}$, and 0.94 ± 0.23, respectively, when input uncertainties are the standard uncertainty (Eq. 1). When the input uncertainty for pH^{est} is only the RMSE of 0.0161 (Sect. 3.1), uncertainties decrease to $\pm 98\,\mu\text{mol}\,\text{kg}^{-1}$, $\pm 93\,\mu\text{mol}\,\text{kg}^{-1}$, and ±0.09, respectively. When input uncertainties are only the random component of the input parameters (i.e., standard deviation for pH_{SeaFET} and pCO_2 and instrument precision for T and S), TA(pH_{SeaFET}, pCO_2), DIC(pH_{SeaFET}, pCO_2), and Ω_{arag}(pH_{SeaFET}, pCO_2) u_c drops to $\pm 38\,\mu\text{mol}\,\text{kg}^{-1}$, $\pm 37\,\mu\text{mol}\,\text{kg}^{-1}$, and ±0.06, respectively. Given the above uncertainties and that we do not see significant biofouling at the CEO site, we believe that short-term variability can be discussed with confidence with this dataset. In other words, wiggles in the data represent real events, despite the high uncertainty in the precise value of the calculated parameters.

4.3 Subsurface biogeochemical drivers of pH, Ω_{arag}, and pCO_2

Inorganic carbon chemistry can be influenced by advection and vertical entrainment of different water masses, temperature, salinity, biogeochemistry, and conservative mixing with TA and DIC freshwater endmembers. Here, we followed Rheuban et al. (2019) and separated the drivers of the observed large pH, Ω_{arag}, and pCO_2 variability to provide additional insights into our time series (Fig. 10) using CO2SYS by altering the input parameters temperature, salinity, TA, and DIC. Anomalies (black) relative to the reference values pH(T_0, S_0, DIC_0, TA_0), Ω_{arag}(T_0, S_0, DIC_0, TA_0), and pCO_2(T_0, S_0, DIC_0, TA_0) were calculated using a linear Taylor series decomposition, adding up the thermodynamic effects of temperature and salinity and the perturbations due to biogeochemistry and conservative mixing with freshwater DIC and TA endmembers (Rheuban et al., 2019). Reference values T_0, S_0, DIC_0, and TA_0, are the mean of the CEO time series. Freshwater from sea ice melt and meteoric sources (precipitation and rivers) may influence the CEO site. TA and DIC concentrations of 450 and $400\,\mu\text{mol}\,\text{kg}^{-1}$, respectively, have been measured in Arctic sea ice (Rysgaard et al., 2007). Riverine input along the Gulf of Alaska tends to have lower TA ($366\,\mu\text{mol}\,\text{kg}^{-1}$) and DIC ($397\,\mu\text{mol}\,\text{kg}^{-1}$) concentrations (Stackpoole et al., 2016, 2017) than rivers draining into the Bering, Chukchi, and Beaufort seas ($TA = 1860\,\mu\text{mol}\,\text{kg}^{-1}$, $DIC = 2010\,\mu\text{mol}\,\text{kg}^{-1}$; Holmes et al., 2021) all of which can influence the CEO site to some extent (Asahara et al., 2012; Jung et al., 2021). In this Taylor decomposition we used sea ice TA and DIC endmembers (Rysgaard et al., 2007) but want to emphasize that using Arctic river endmembers did not meaningfully change the results (not shown). Figure 10 shows the effects of biogeochemical processes, temperature, salinity, and conservative mixing with TA and DIC freshwater endmembers on pH, Ω_{arag}, and pCO_2. The effects of salinity (turquoise) and conservative mixing with TA and DIC freshwater endmembers (green) are negligible for pH, Ω_{arag}, and pCO_2. Temperature varied between −1.7 °C during the sea-ice-covered months and up to 4 °C in late fall, when wind events mixed the whole water column and entrained warm and low-pCO_2 surface waters to the instrument depth at 33 m (see Sect. 3.2 for a more in-depth discussion of these mixing events). During this time, the increase in temperature counteracted the effect of biogeochemistry slightly and increased pCO_2 and decreased pH (Fig. 10a, c). Temperature did not affect Ω_{arag}.

Biogeochemistry (photosynthesis, respiration, calcification, dissolution) is the most important driver of the inorganic carbon dynamics at 33 m depth at the CEO site. The springtime relaxation events in 2018 and 2019 with relatively higher pH and Ω_{arag} and lower pCO_2 were mainly driven by biogeochemistry (Fig. 10, magenta). During these events O_2 increased and NO_3 decreased, suggesting photosynthetic ac-

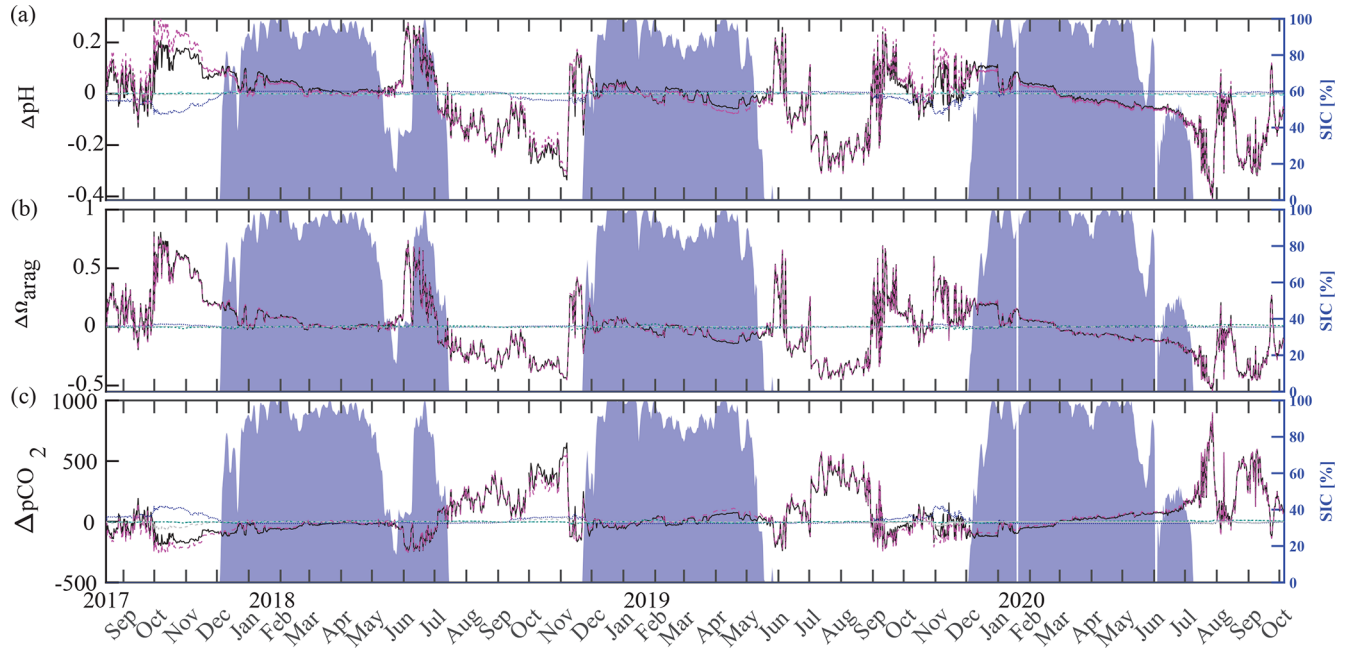

Figure 10. Drivers of the inorganic carbon system. Component time series of the linear Taylor decomposition of **(a)** pH, **(b)** Ω_{arag}, and **(c)** pCO_2. Contributions of changes in salinity (turquoise), temperature (blue), biogeochemistry (pink), and freshwater mixing (green) to changes (black, relative to the mean of the time series) in pH, Ω_{arag}, and pCO_2 were computed following Rheuban et al. (2019). The gray dotted line illustrates an estimated residual term. Sea ice concentration (blue shading, %; DiGirolamo et al., 2022) is shown on the right axes.

tivity (Figs. 2d, e and 3a). Near-bottom photosynthetic activity by phytoplankton or sea ice algae has been observed at different locations across the Chukchi Sea (Arrigo et al., 2017; Ouyang et al., 2022; Stabeno et al., 2020; Koch et al., 2020). Sediment trap data from a CEO deployment prior to the start of this pCO_2 and pH time series suggest that export of the exclusively sympagic sea ice algae *Nitzschia frigida* peaked in May and June, during snowmelt and ice melt events (Lalande et al., 2020), further supporting the hypothesis that sea ice algae contributed to the CO_2 drawdown. Interestingly, TA also increased significantly during these events in 2018 and 2019, which cannot be solely attributed to organic-matter production. Specifically, TA increased by 23 µmol kg^{-1} in 2019 (Fig. 11a). However, with an observed NO_3 decrease of 7.6 µmol kg^{-1}, we would expect an increase in TA by 7.6 µmol kg^{-1}. This is assuming that NO_3 is the primary source of nitrogen during organic-matter formation and that assimilation of 1 µmol of NO_3 leads to an increase in TA of 1 µmol (Wolf-Gladrow et al., 2007). The TA increase of 23 µmol kg^{-1} is therefore larger than expected from organic-matter formation alone and is likely due to $CaCO_3$ mineral dissolution. While direct evidence is missing, the strong TA increase suggests that $CaCO_3$ mineral dissolution during sea ice break-up also plays an important role at the CEO site. As observed in other Arctic areas, it is possible that ikaite crystals that were trapped in the ice matrix dissolved in the water column when sea ice melted (Rysgaard et al., 2012, 2007).

4.4 Progression of ocean acidification in the Chukchi Sea

Organisms living at the CEO site may have always been exposed to large seasonal variability and low pH and Ω_{arag} (high pCO_2), but the combined and cumulative effects of climate change and ocean acidification have rapidly made these conditions more extreme and longer lasting. Ocean acidification serves as a gradual environmental press by increasing the system's mean and extreme pCO_2 and decreasing mean and extreme pH and Ω_{arag}. Climate-induced changes to other important controls of the inorganic carbon system, such as sea ice, riverine input, temperature, and circulation can act as sudden pulses and further modulate the inorganic carbon system to a less predictable degree and cause extreme events (Woosley and Millero, 2020; Orr et al., 2022; Hauri et al., 2021; Qi et al., 2017). Huntington et al. (2020) describe a sudden and dramatic shift of the physical, biogeochemical, and ecosystem conditions in the Chukchi and northern Bering seas in 2017. For example, satellite data for the CEO site illustrate that the longest open-water seasons on record occurred between 2017 and 2020. Before 2017, the open-water season was on average 81 (±40) d long (i.e., below 15 % concentration), of which 60 (±44) d were ice free, whereas between 2017 and 2020, the low-sea-ice period was 157 (±30) d long, of which 152 (±24) d were ice free (Fig. 12). Sea ice decline and increased nutrient influx has also promoted increased phytoplankton primary produc-

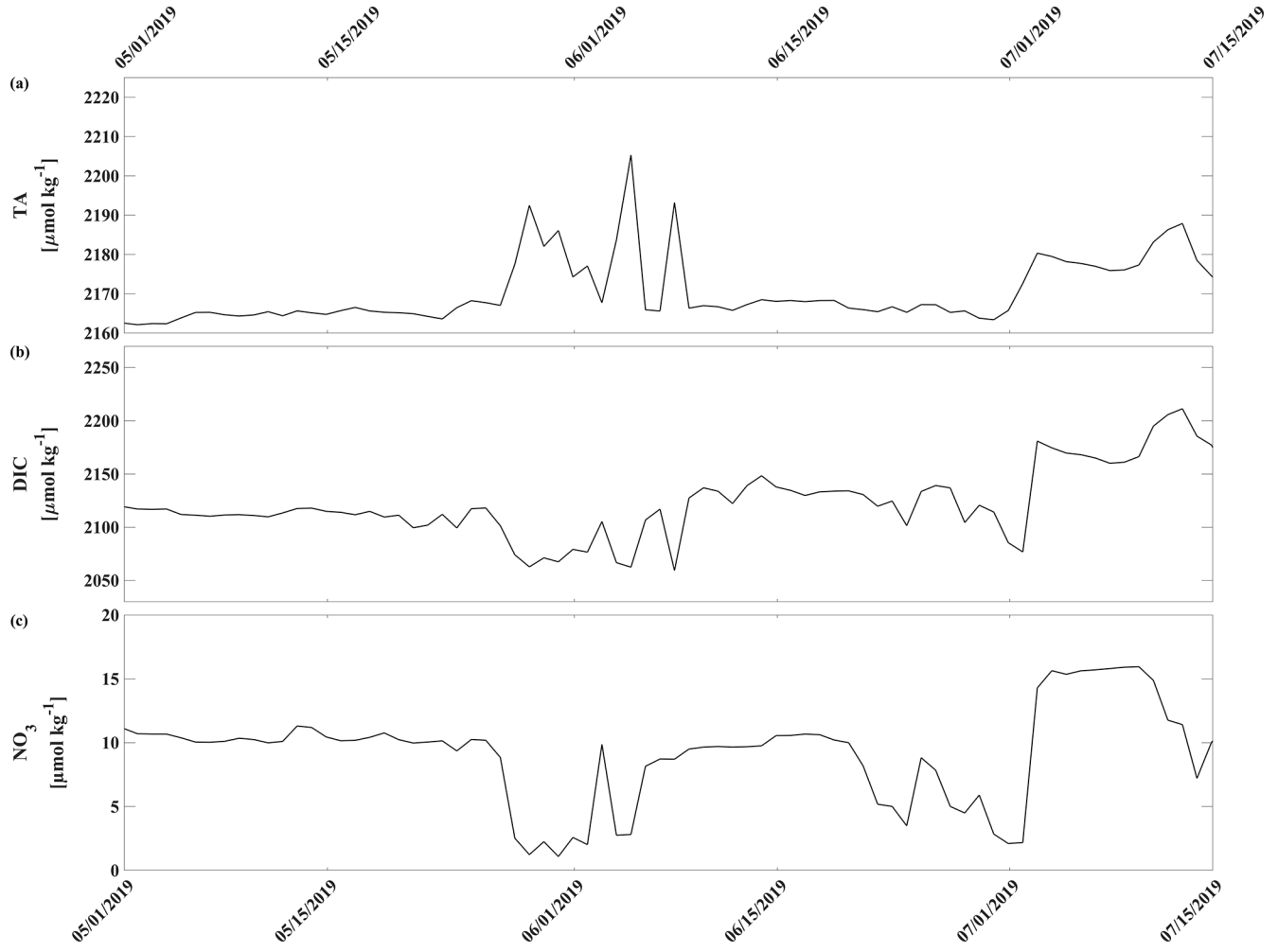

Figure 11. Spring 2019 relaxation event. Time series of **(a)** total alkalinity (TA, µmol kg^{-1}), **(b)** dissolved inorganic carbon (DIC, µmol kg^{-1}), and **(c)** nitrate (NO_3, µmol kg^{-1}) from 1 May through 15 July 2019.

tion in the area (Lewis et al., 2020; Arrigo and van Dijken, 2015; Payne et al., 2021). Since our inorganic carbon time series started after the "dramatic shift" that was observed in the Chukchi Sea in 2017 (Huntington et al., 2020) and given the uncertainty in model output in this region, we can only speculate about how the changes in sea ice, temperature, and biological production may have affected seasonal variability and extremes of the inorganic carbon chemistry at the CEO site. However, since the summertime low pH and Ω_{arag} and high pCO_2 are tightly coupled to the length of the ice-free period and intensity of organic-matter production, it is possible that the observed summertime period of extreme conditions may have been previously unexperienced at this site. We therefore think it is justified to call the spikes in pH and Ω_{arag} "ocean acidification relaxation events", since the long-lasting summertime period of extremely low pH and Ω_{arag} may be a new pattern.

4.5 Relevance for ecosystem

Marine organisms are exposed to a wide range of naturally fluctuating environmental conditions such as temperature, salinity, carbonate chemistry, and food concentrations that together constitute their ecological niche. As evolution works toward adaptation, the tolerance range of species and ecosystems to such parameters varies between locations and is often closely related to niche status (Vargas et al., 2022). Stress can be defined as a condition evoked in an organism by one or more environmental and biological factors that bring the organism near or over the limits of its ecological niche (after Van Straalen, 2003). The consequence of the exposure to a stressor will depend on organismal sensitivity, stress intensity (how much it deviates from present conditions), and stress duration. In a synthesis of the global literature on the biological impacts of ocean acidification, Vargas et al. (2017, 2022) showed that the extreme of the present range of variability of carbonate chemistry is a good predictor of species

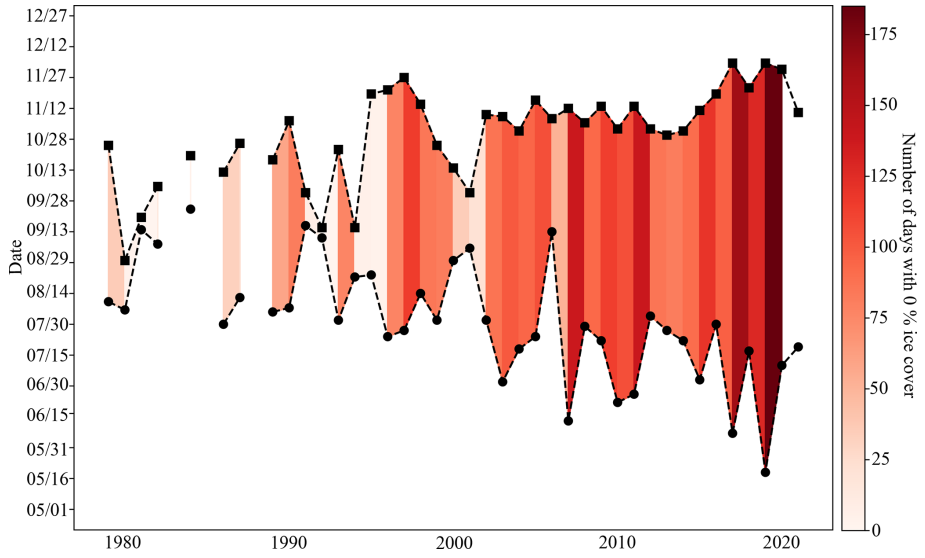

Figure 12. Low-sea-ice period at the Chukchi Sea Observatory. Time series of start (circle) and end (square) of low sea ice (< 15 % per grid cell) period from 1982–2021. Shades of red illustrate the number of days with 0 % sea ice cover. The satellite sea ice cover at the observatory site was taken from the NSIDC (DiGirolamo et al., 2022).

sensitivity. In other words, larger deviations from present extreme high pCO_2 or extreme low pH, would be expected to exert more negative biological impacts. Organismal stress and niche boundaries have implications for the definition and understanding of controls and future ocean acidification conditions in experiments aimed at evaluating future biological impacts.

Our data provide insights into conditions that affect and determine local species' ecological niches, and a necessary key is to evaluate or re-evaluate their sensitivity to present and future carbonate chemistry conditions, particularly for the sessile benthic calcifiers that constitute prey for mobile and upper trophic-level taxa. For example, an experimental study on three common Arctic bivalve species (*Macoma calcarea*, *Astarte montagui* and *Astarte borealis*) collected in the CEO concluded that these species were generally resilient to decreasing pH (Goethel et al., 2017). However, only two pH values were compared (a "control" (pH of 8.1) and an "acidified" treatment (pH of 7.8)) and our results show that organisms are already experiencing more extreme conditions today than have been experimentally manipulated. While these data provide insights into these species' plasticity to present pH conditions, they cannot be used to infer sensitivity to future ocean acidification or extremes of current conditions. Based on the local adaptation hypothesis (Vargas et al., 2017, 2022), stress and the associated negative effect on species fitness can be expected when pH deviates from the extreme of the present range of variability (pH < 7.5) as shown in other regions (e.g., echinoderms: Dorey et al., 2013; crustaceans: Thor and Dupont, 2015; bivalves: Ventura et al., 2016).

At the CEO, our results show sustained periods of remarkably low pH (e.g., 7.5; summer to fall, winter). Higher pH values are observed in spring and late fall. While we are lacking the local biological data to sufficiently evaluate past and future ecosystem changes, a high rate of ocean acidification as observed in the Chukchi Sea (Qi et al., 2022a, b), associated with potential temperature-induced shifts in the carbonate chemistry cycle (e.g., Orr et al., 2022), has the potential to impact species and ecosystems. Exposure to low pH increases organismal energy requirements for maintenance (e.g., acid–base regulation: Stumpp et al., 2012; compensatory calcification: Ventura et al., 2016). Organisms can cope with increased energy costs using a variety of strategies, ranging from individual physiological to behavioral responses, depending on trophic level, mobility, and other ecological factors. For example, they can use available stored energy to compensate for increased costs or they can decrease their metabolism to limit costs (AMAP, 2018). At the CEO, the low-pH period observed during the summer and fall is associated with elevated temperature and an elevated food supply for herbivores (Lalande et al., 2020). The high availability of food may then foster compensation for the higher energetic costs associated with exposure to low pH. However, a longer period of low pH as suggested by our data could lead to a mismatch between the low pH and food availability, with cascading negative consequences for the ecosystem (Kroeker et al., 2021). In winter, the low-pH conditions are associated with low temperature, no light, and low food level concentrations. These conditions are likely to keep metabolisms low and limit the negative effects of exposure to low pH (Gianguzza et al., 2014). As food availability is limited by the absence of light, this strategy may be compromised by an increase in temperature that could also lead to increased metabolism. Additional work is needed to under-

stand the impacts of acidification conditions and variability on the marine biota of the Chukchi Sea, including field and laboratory experiments that evaluate the biological response under realistic scenarios. The characterization of the environmental conditions at the CEO, including the variability in time, can be used to design single- and multiple-stressor experiments (carbonate chemistry, temperature, salinity, food, oxygen; Boyd et al., 2018).

Indigenous communities are at the forefront of the changing Arctic, including changes in accessibility, availability, and the condition of traditional marine foods (Buschman and Sudlovenick, 2022; Hauser et al., 2021). Several marine species are critical to the food and cultural security of coastal Iñupiat, who have thrived in Arctic Alaska for millennia. While it is not possible to resolve the consequences of the seasonal and interannual variations in carbonate chemistry documented in this paper without a proper sensitivity evaluation, the seasonally low-pH conditions have the potential to impact organisms like bivalves in a foraging hotspot for walrus (Jay et al., 2012; Kuletz et al., 2015). Walrus, as well as their bivalve stomach contents, are important nutritional, spiritual, and cultural components, raising concerns for food security in the context of ecosystem shifts associated with the variability and multiplicity of climate impacts within the region (ICC, 2015).

5 Concluding thoughts

The Chukchi Sea is undergoing a rapid environmental transformation with potentially far-reaching consequences across the ecosystem. While we are lacking a long-term time series, we used this dataset to investigate the drivers of extreme pH, Ω_{arag}, and pCO_2 and document conditions that could affect the ecological niches of organisms, including a fast rate of ocean acidification, elongated sea-ice-free periods, increased primary productivity, and elevated temperature. While a combination of experimental and monitoring approaches is needed for an understanding of the ecological consequences of these changes, our results also highlight the urgency to mitigate CO_2 emissions and simultaneously support Indigenous-led conservation measures to safeguard an ecosystem in transition. Indigenous People in the Arctic have established strategies to monitor, adapt to, and conserve the ecosystems upon which they depend. Ethical and equitable engagement of Indigenous Knowledge and the communities at the forefront of climate impacts can help guide research and conservation action by centering local priorities and traditional practices, thereby supporting self-determination and sovereignty (Buschman and Sudlovenick, 2022).

Code availability. Scripts that are interlinked to process NO_3 data are available at https://github.com/britairving/SUNA_V2_processing (Irving, 2021).

Data availability. The inorganic carbon data used in this paper are publicly available (https://doi.org/10.24431/rw1k7dq and https://doi.org/10.24431/rw1k7dp; Hauri and Irving, 2023a, b).

Supplement. The supplement related to this article is available online at: https://doi.org/10.5194/bg-21-1135-2024-supplement.

Author contributions. CH and BI managed and serviced the HydroC CO_2 and SeapHOx sensors, analyzed and published the data, and wrote the paper. SD carried out the CEO mooring deployments and recoveries and managed and serviced the CTD and NO_3 sensors. RP, DDWH, SD, and SLD contributed to the paper.

Competing interests. The contact author has declared that none of the authors has any competing interests.

Disclaimer. Publisher's note: Copernicus Publications remains neutral with regard to jurisdictional claims made in the text, published maps, institutional affiliations, or any other geographical representation in this paper. While Copernicus Publications makes every effort to include appropriate place names, the final responsibility lies with the authors.

Acknowledgements. The Chukchi Ecosystem Observatory is located on the traditional and contemporary hunting grounds of the northern Alaska Iñupiat. We also acknowledge that our Fairbanks-based offices are located on the Native lands of the Lower Tanana Dena. The Indigenous Peoples of this land never surrendered lands or resources to Russia or the United States. We acknowledge this not only because we are grateful to the Indigenous communities, who have been in deep connection with the land and water for time immemorial, but also in recognition of the historical and ongoing legacy of colonialism. We are committed to improving our scientific approaches and working towards co-production for a better future for everyone.

We acknowledge the World Climate Research Programme, which, through its Working Group on Coupled Modelling, coordinated and promoted CMIP6. We thank the climate modeling groups for producing and making available their model output, the Earth System Grid Federation (ESGF) for archiving the data and providing access, and the multiple funding agencies who support CMIP6 and ESGF. We would also like to express our thanks for the valuable input from two anonymous reviewers and the editor as well as Lauren Barrett and Melissa Chierici, who both reviewed the paper. Maintenance and calibration of the CEO sensors is only possible due to the kind support of numerous collaborators within the Arctic research community who helped with CEO deployment and recovery or collected sensor calibration samples. We would therefore like to thank Peter Shipton, Carin Ashjian, Jessica Cross, Miguel Goñi, Jackie Grebmeier, Burke Hales, Katrin Iken, Laurie Juranek, Calvin Mordy, and Robert Pickart. The International Atomic Energy Agency is grateful to the Government of the Principality of Monaco for the support provided to its Marine Environment Laboratories.

Financial support. The authors received financial support from the National Pacific Research Board Long-term Monitoring (NPRB LTM) program (project nos. 1426 and L-36), the Alaska Ocean Observing System (award nos. NA11NOS0120020 and NA16NOS0120027), and the University of Alaska Fairbanks. Claudine Hauri, Brita Irving, and Seth Danielson also received support from the National Science Foundation Office of Ocean Sciences and Polar Programs (grant nos. OCE-1841948 and OPP-1603116). Projects that assisted in the servicing of the CEO and/or collected water column calibration data were funded by the National Science Foundation, Bureau of Ocean Energy Management, National Oceanic and Atmospheric Administration, National Oceanographic Partnership Program, and Shell Exploration and Production Company, Inc. Moreover, Donna Houser received support from the Alaska Arctic Observatory and Knowledge Hub.

Review statement. This paper was edited by Olivier Sulpis and reviewed by two anonymous referees.

References

Alin, S. R., Feely, R. A., Dickson, A. G., Hernández-Ayón, J. M., Juranek, L. W., Ohman, M. D., and Goericke, R.: Robust empirical relationships for estimating the carbonate system in the southern California Current System and application to CalCOFI hydrographic cruise data (2005–2011), J. Geophys. Res., 117, C05033, https://doi.org/10.1029/2011JC007511, 2012.

AMAP: AMAP Assessment 2018: Arctic Ocean Acidification, Arctic Monitoring and Assessment Programme (AMAP), Tromsø, Norway, vi+187 pp., https://www.amap.no/documents/doc/AMAP-Assessment-2018-Arctic-Ocean-Acidification/1659 (last access: 10 April 2022), 2018.

Arrigo, K. R. and van Dijken, G. L.: Continued increases in Arctic Ocean primary production, Prog. Oceanogr., 136, 60–70, https://doi.org/10.1016/j.pocean.2015.05.002, 2015.

Arrigo, K. R., Mills, M. M., van Dijken, G. L., Lowry, K. E., Pickart, R. S., and Schlitzer, R.: Late Spring Nitrate Distributions Beneath the Ice-Covered Northeastern Chukchi Shelf, J. Geophys. Res.-Biogeo., 122, 2409–2417, https://doi.org/10.1002/2017JG003881, 2017.

Asahara, Y., Takeuchi, F., Nagashima, K., Harada, N., Yamamoto, K., Oguri, K., and Tadai, O.: Provenance of terrigenous detritus of the surface sediments in the Bering and Chukchi Seas as derived from Sr and Nd isotopes: Implications for recent climate change in the Arctic regions, Deep-Sea Res. Pt. II, 61–64, 155–171, https://doi.org/10.1016/j.dsr2.2011.12.004, 2012.

Bates, N.: Assessing ocean acidification variability in the Pacific-Arctic region as part of the Russian-American Long-term Census of the Arctic, Oceanography, 28, 36–45, https://doi.org/10.5670/oceanog, 2015.

Bates, N. R., Mathis, J. T., and Cooper, L. W.: Ocean acidification and biologically induced seasonality of carbonate mineral saturation states in the western Arctic Ocean, J. Geophys. Res., 114, C11007, https://doi.org/10.1029/2008JC004862, 2009.

Bednaršek, N., Calosi, P., Feely, R. A., Ambrose, R., Byrne, M., Chan, K. Y. K., Dupont, S., Padilla-Gamiño, J. L., Spicer, J. I., Kessouri, F., Roethler, M., Sutula, M., and Weisberg, S. B.: Synthesis of thresholds of ocean acidification impacts on echinoderms, Front. Mar. Sci., 8, 602601, https://doi.org/10.3389/fmars.2021.602601, 2021.

Bittig, H. C., Steinhoff, T., Claustre, H., Fiedler, B., Williams, N. L., Sauzède, R., Körtzinger, A., and Gattuso, J.-P.: An alternative to static climatologies: robust estimation of open ocean CO_2 variables and nutrient concentrations from T, S, and O_2 data using Bayesian neural networks, Front. Mar. Sci., 5, 328, https://doi.org/10.3389/fmars.2018.00328, 2018.

Blanchard, A. L., Parris, C. L., Knowlton, A. L., and Wade, N. R.: Benthic ecology of the northeastern Chukchi Sea. Part I. Environmental characteristics and macrofaunal community structure, 2008–2010, Cont. Shelf Res., 67, 52–66, 2013.

Boucher, O., Denvil, S., Levavasseur, G., Cozic, A., Caubel, A., Foujols, M.-A., Meurdesoif, Y., Balkanski, Y., Checa-Garcia, R., Hauglustaine, D., Bekki, S., and Marchand, M.: IPSL IPSL-CM6A-LR-INCA model output prepared for CMIP6 AerChemMIP, Earth System Grid Federation, https://doi.org/10.22033/ESGF/CMIP6.13581, 2020.

Boyd, P. W., Collins, S., Dupont, S., Fabricius, K., Gattuso, J.-P., Havenhand, J., Hutchins, D. A., Riebesell, U., Rintoul, M. S., Vichi, M., Biswas, H., Ciotti, A., Gao, K., Gehlen, M., Hurd, C. L., Kurihara, H., McGraw, C. M., Navarro, J. M., Nilsson, G. E., Passow, U., and Pörtner, H.-O.: Experimental strategies to assess the biological ramifications of multiple drivers of global ocean change – A review, Glob. Change Biol., 24, 2239–2261, 2018.

Breitberg, D., Salisbury, J., Bernhard, J., Cai, W.-J., Dupont, S., Doney, S., Kroeker, K., Levin, L. A., Long, W. C., Milke, L. M., Miller S. H., Phelan, B., Passow, U., Seibel, B. A., Todgham, A. E., and Tarrant, A. M.: And on top of all that… Coping with ocean acidification in the midst of many stressors, Oceanography, 25, 48–61, https://doi.org/10.5670/oceanog.2015.31, 2015.

Bresnahan, P. J., Martz, T. R., Takeshita, Y., Johnson, K. S., and LaShomb, M.: Best practices for autonomous measurement of seawater pH with the Honeywell Durafet, Methods Oceanogr., 9, 44–60, https://doi.org/10.1016/j.mio.2014.08.003, 2014.

Brodzik, M. J. and Knowles, K. W.: Chapter 5: EASE-Grid: A Versatile Set of Equal-Area Projections and Grids, in: Discrete Global Grids: A Web Book, edited by: Goodchild, M. F., Santa Barbara, California USA, National Center for Geographic Information & Analysis, https://escholarship.org/uc/item/9492q6sm (last access: 25 February 2023), 2002.

Buschman, V. Q. and Sudlovenick, E.: Indigenous-led conservation in the Arctic supports global conservation practices, Arctic Sci., 9, 714–719, https://doi.org/10.1139/as-2022-0025, 2022.

Carmack, E. and Wassmann, P.: Food webs and physical–biological coupling on pan-Arctic shelves: unifying concepts and comprehensive perspectives, Prog. Oceanogr., 71, 446–477, 2006.

Carter, B. R., Feely, R. A., Williams, N. L., Dickson, A. G., Fong, M. B., and Takeshita, Y.: Updated methods for global locally interpolated estimation of alkalinity, pH, and nitrate, Methods Limnology and Oceanography, 16, 119–131, https://doi.org/10.1002/lom3.10232, 2018.

Chatterjee, S. and Hadi, A. S.: Influential Observations, High Leverage Points, and Outliers in Linear Regression, Stat. Sci., 1, 379–416, https://doi.org/10.1214/ss/1177013622, 1986.

Corlett, W. B. and Pickart, R. S.: The Chukchi slope current, Prog. Oceanogr., 153, 50–65, 2017.

Cross, J. N., Monacci, N. M., Bell, S. W., Grebmeier, J. M., Mordy, C., Pickart, R. S., and Stabeno, P. J.: Dissolved inorganic carbon (DIC), total alkalinity (TA) and other variables collected from discrete samples and profile observations from United States Coast Guard Cutter (USCGC) Healy cruise HLY1702 (EXPOCODE 33HQ20170826) in the Bering and Chukchi Sea along transect lines in the Distributed Biological Observatory (DBO) from 2017-08-26 to 2017-09-15 (NCEI Accession 0208337), NOAA National Centers for Environmental Information [data set], https://doi.org/10.25921/pks4-4p43, 2020a.

Cross, J. N., Monacci, N. M., Bell, S. W., Grebmeier, J. M., Mordy, C., Pickart, R. S., and Stabeno, P. J.: Dissolved inorganic carbon (DIC), total alkalinity (TA) and other parameters collected from discrete sample and profile observations during the USCGC Healy cruise HLY1801 (EXPOCODE 33HQ20180807) in the Bering Sea, Chukchi Sea and Beaufort Sea along transect lines in the Distributed Biological Observatory (DBO) from 2018-08-07 to 2018-08-24 (NCEI Accession 0221911), NOAA National Centers for Environmental Information [data set], https://doi.org/10.25921/xc4b-xh20, 2020b.

Cross, J. N., Monacci, N. M., Bell, S. W., Grebmeier, J. M., Mordy, C., Pickart, Robert S., and Stabeno, P. J.: Dissolved inorganic carbon (DIC) and total alkalinity (TA) and other hydrographic and chemical data collected from discrete sample and profile observations during the United States Coast Guard Cutter (USCGC) Healy cruise HLY1901 (EXPOCODE 33HQ20190806) in the Bering and Chukchi Sea along transect lines in the Distributed Biological Observatory (DBO) from 2019-08-06 to 2019-08-22 (NCEI Accession 0243277). NOAA National Centers for Environmental Information [data set], https://doi.org/10.25921/b5s5-py61, 2021.

Cullison-Gray, S. E., DeGrandpre, M. D., Moore, T. S., Martz, T. R., Friederich, G. E., and Johnson, K. S.: Applications of in situ pH measurements for inorganic carbon calculations, Mar. Chem., 125, 82–90, https://doi.org/10.1016/j.marchem.2011.02.005, 2011.

Daniel, A., Laës-Huon, A., Barus, C., Beaton, A. D., Blandfort, D., Guigues, N., Knockaert, M., Munaron, D., Salter, I., Woodward, E. M. S., Greenwood, N., and Achterberg, E. P.: Toward a harmonization for using in situ nutrient sensors in the marine environment, Front. Mar. Sci., 6, 773, https://doi.org/10.3389/fmars.2019.00773, 2020.

Danielson, S. L., Iken, K., Hauri, C., Hopcroft, R. R., McDonnell, A. M., Winsor, P., Lalande, C., Grebmeier, J. M., Cooper, L. W., Horne, J. K., and Stafford, K. M.: Collaborative approaches to multi-disciplinary monitoring of the Chukchi shelf marine ecosystem: Networks of networks for maintaining long-term Arctic observations, in: OCEANS 2017-Anchorage, 1–7, IEEE, 2017.

Danielson, S. L., Ahkinga, O., Ashjian, C., Basyuk, E., Cooper, L. W., Eisner, L., Farley, E., Iken, K. B., Grebmeier, J. M., Juranek, L., Khen, G., Jayne, S. R., Kikuchi, T., Ladd, C., Lu, K., McCabe, R. M., Moore, G. W. K., Nishino, S., Ozenna, F., Pickart, R. S., Polyakov, I., Stabeno, P. J., Thoman, R., Williams, W. J., Wood, K., and Weingartner, T. J.: Manifestation and consequences of warming and altered heat fluxes over the Bering and Chukchi Sea continental shelves, Deep-Sea Res. Pt. II, 177, 104781, https://doi.org/10.1016/j.dsr2.2020.104781, 2020.

DeGrandpre, M. D., Lai, C.-Z., Timmermans, M.-L., Krishfield, R. A., Proshutinsky, A., and Torres, D.: Inorganic Carbon and pCO_2 Variability During Ice Formation in the Beaufort Gyre of the Canada Basin, J. Geophys. Res.-Oceans, 124, 4017–4028, 2019.

Dickson, A. G.: Thermodynamics of the dissociation of boric acid in synthetic seawater from 273.15 to 318.15 K, Deep-Sea Res. Pt. A, 37, 755–766, https://doi.org/10.1016/0198-0149(90)90004-F, 1990.

Dickson, A. G., Sabine, C. L., and Christian, J. R.: Guide to best practices for ocean CO_2 measurements, PICES, Sydney, 191 pp., https://www.nodc.noaa.gov/ocads/oceans/Handbook_2007.html (last access: 5 March 2024), 2007.

DiGirolamo, N. E., Parkinson, C. L., Cavalieri, D. J., Gloersen, P., and Zwally, H. J.: Sea Ice Concentrations from Nimbus-7 SMMR and DMSP SSM/I-SSMIS Passive Microwave Data, Version 2, Boulder, Colorado USA, NASA National Snow and Ice Data Center Distributed Active Archive Center, https://doi.org/10.5067/MPYG15WAA4WX, 2022.

Dorey, N., Lançon, P., Thorndyke, M., and Dupont, S.: Assessing physiological tipping point of sea urchin larvae exposed to a broad range of pH, Glob. Change Biol., 19, 3355–3367, https://doi.org/10.1111/gcb.12276, 2013.

Doney, S. C., Busch, D. S., Cooley, S. R., and Kroeker, K. J.: The Impacts of Ocean Acidification on Marine Ecosystems and Reliant Human Communities, Annu. Rev. Env. Resour., 45, 83–112, 2020.

Duke, P. J., Else, B. G. T., Jones, S. F., Marriot, S., Ahmed, M. M. M., Nandan, V., Butterworth, B., Gonski, S. F., Dewey, R., Sastri, A., Miller, L. A., Simpson, K. G., and Thomas, H.: Seasonal marine carbon system processes in an Arctic coastal landfast sea ice environment observed with an innovative underwater sensor platform, Elementa, 9, 00103, https://doi.org/10.1525/elementa.2021.00103, 2021.

Fang, Y. C., Weingartner, T. J., Dobbins, E. L., Winsor, P., Statscewich, H., Potter, R. A., Mudge, T. D., Stoudt, C. A., and Borg, K.: Circulation and thermohaline variability of the Hanna Shoal region on the northeastern Chukchi Sea shelf, J. Geophys. Res.-Oceans, 125, e2019JC015639, https://doi.org/10.1029/2019JC015639, 2020.

Fietzek, P., Fiedler, B., Steinhoff, T., and Körtzinger, A.: In situ quality assessment of a novel underwater CO_2 sensor based on membrane equilibration and NDIR spectrometry, J. Atmos. Ocean. Tech., 31, 181–196, https://doi.org/10.1175/JTECH-D-13-00083.1, 2014.

Gianguzza, P., Visconti, G., Gianguzza, F., Vizzini, S., Sarà, G., and Dupont, S.: Temperature modulates the response of the thermophilous sea urchin Arbacia lixula early life stages to CO_2-driven acidification, Mar. Environ. Res., 93, 70–77, https://doi.org/10.1016/j.marenvres.2013.07.008, 2014.

Goethel, C. L., Grebmeier, J. M., Cooper, L. W., and Miller, T. J.: Implications of ocean acidification in the Pacific Arctic: Experimental responses of three Arctic bivalves to decreased pH and food availability, Deep-Sea Res. Pt. II, 144, 112–124, https://doi.org/10.1016/j.dsr2.2017.08.013, 2017.

Gonzalez, S., Horne, J. K., and Danielson, S. L.: Multi-scale temporal variability in biological-physical associations in the NE Chukchi Sea, Polar Biol., 44, 837–855, https://doi.org/10.1007/s00300-021-02844-1, 2021.

Grebmeier, J. M., Bluhm, B. A., Cooper, L. W., Danielson, S. L., Arrigo, K. R., Blanchard, A. L., Clarke, J. T., Day, R. H., Frey, K. E., Gradinger, R. R., Kędra, M., Konar, B., Kuletz, K. J., Lee, S. H., Lovvorn, J. R., Norcross, B. L., and Okkonen, S. R.: Ecosystem characteristics and processes facilitating persistent macrobenthic biomass hotspots and associated benthivory in the Pacific Arctic, Prog. Oceanogr., 136, 92–114, https://doi.org/10.1016/j.pocean.2015.05.006, 2015.

Hauri, C. and Irving, B.: pCO_2 time series measurements from the Chukchi Ecosystem Observatory CEO2 mooring deployed at 33 meters depth in the Northeast Chukchi Sea, version: 10.24431_rw1k7dq_20230531T123002Z, Research Workspace [data set], https://doi.org/10.24431/rw1k7dq, 2023a.

Hauri, C. and Irving, B.: pH, temperature, salinity, and oxygen time series measurements from the Chukchi Ecosystem Observatory CEO2 mooring deployed at 33 meters depth in the Northeast Chukchi Sea, version: 10.24431_rw1k7dp_20230531T121136Z, Research Workspace [data set], https://doi.org/10.24431/rw1k7dp, 2023b.

Hauri, C., Gruber, N., Vogt, M., Doney, S. C., Feely, R. A., Lachkar, Z., Leinweber, A., McDonnell, A. M. P., Munnich, M., and Plattner, G.-K.: Spatiotemporal variability and long-term trends of ocean acidification in the California Current System, Biogeosciences, 10, 193–216, https://doi.org/10.5194/bg-10-193-2013, 2013.

Hauri, C., Danielson, S., McDonnell, A. M. P., Hopcroft, R. R., Winsor, P., Shipton, P., Lalande, C., Stafford, K. M., Horne, J. K., Cooper, L. W., Grebmeier, J. M., Mahoney, A., Maisch, K., McCammon, M., Statscewich, H., Sybrandy, A., and Weingartner, T.: From sea ice to seals: a moored marine ecosystem observatory in the Arctic, Ocean Sci., 14, 1423–1433, https://doi.org/10.5194/os-14-1423-2018, 2018.

Hauri, C., Pagès, R., McDonnell, A. M. P., Stuecker, M. F., Danielson, S. L., Hedstrom, K., Irving, B., Schultz, C., and Doney, S. C.: Modulation of ocean acidification by decadal climate variability in the Gulf of Alaska, Commun. Earth Environ, 2, 191, https://doi.org/10.1038/s43247-021-00254-z, 2021.

Hauser, D. D. W., Whiting, A. V., Mahoney, A. R., Goodwin, J., Harris, C., Schaeffer, R. J., Schaeffer, R., Laxague, N. J. M., Subramaniam, A., Witte, C. R., Betcher, S., Lindsay, J. M., and Zappa, C. J.: Co-production of knowledge reveals loss of Indigenous hunting opportunities in the face of accelerating Arctic climate change, Environ. Res. Lett., 16, 095003, https://doi.org/10.1088/1748-9326/ac1a36, 2021.

Hayes, D., Kemme, J., and Hauri C.: Ocean greenhouse gas monitoring: new autonomous platform to measure pCO_2, methane, Sea Technol., 63, 13–16, https://lsc-pagepro.mydigitalpublication.com/publication/?i=764237&p=13&view=issueViewer (last access: 25 July 2023), 2022.

Hennon, T. D., Danielson, S. L., Woodgate, R. A., Irving, B., Stockwell, D. A., and Mordy, C. W.: Mooring Measurements of Anadyr Current Nitrate, Phosphate, and Silicate Enable Updated Bering Strait Nutrient Flux Estimates, Geophys. Res. Lett., 49, e2022GL098908, https://doi.org/10.1029/2022GL098908, 2022.

Holmes, R. M., McClelland, J. W., Tank, S. E., Spencer, R. G. M., and Shiklomanov, A. I.: Arctic Great Rivers Observatory, Water Quality [data set], https://www.arcticgreatrivers.org/data (last access: 25 January 2023), 2021.

Horowitz, L. W., Naik, V., Sentman, L., Paulot, F., Blanton, C., McHugh, C., Radhakrishnan, A., Rand, K., Vahlenkamp, H., Zadeh, N. T., Wilson, C., Ginoux, P., He, J., John, J. G., Lin, M., Paynter, D. J., Ploshay, J., Zhang, A., and Zeng, Y.: NOAA-GFDL GFDL-ESM4 model output prepared for CMIP6 AerChemMIP hist-1950HC, Earth System Grid Federation, https://doi.org/10.22033/ESGF/CMIP6.8568, 2018.

Huntington, H. P., Danielson, S. L., Wiese, F. K., Baker, M., Boveng, P., Citta, J. J., De Robertis, A., Dickson, D. M. S., Farley, E., George, J. C., Iken, K., Kimmel, D. G., Kuletz, K., Ladd, C., Levine, R., Quakenbush, L., Stabeno, P., Stafford, K. M., Stockwell, D., and Wilson, C.: Evidence suggests potential transformation of the Pacific Arctic ecosystem is underway, Nat. Clim. Change, 10, 342–348, https://doi.org/10.1038/s41558-020-0695-2, 2020.

Huntington, H. P., Zagorsky, A., Kaltenborn, B. P., Shin, H. C., Dawson, J., Lukin, M., Dahl, P. E., Guo, P., and Thomas, D. N.: Societal implications of a changing Arctic Ocean, Ambio, 51, 298–306, https://doi.org/10.1007/s13280-021-01601-2, 2022.

ICC: Alaskan Inuit food security conceptual framework: how to assess the Arctic from an Inuit perspective, Inuit Circumpolar Council-Alaska, Anchorage, Inuit Circumpolar Council, https://doi.org/10.25607/OBP-1695, 2015.

Irving, B.: SUNA_V2_processing, GitHub repository [code], https://github.com/britairving/SUNA_V2_processing (last access: 24 September 2022), 2021.

Islam, F., DeGrandpre, M. D., Beatty, C. M., Timmermanns, M.-L., Krishfield, R. A., Toole, J. M., and Laney, S. R.: Sea surface pCO_2 and O_2 dynamics in the partially ice-covered Arctic Ocean, J. Geophys. Res.-Oceans, 122, 1425–1438, https://doi.org/10.1002/2016JC012162, 2017.

Jay, C. V., Fischbach, A. S., and Kochnev, A. A.: Walrus areas of use in the Chukchi Sea during sparse sea ice cover, Mar. Ecol.-Prog. Ser., 468, 1–13, https://doi.org/10.3354/meps10057, 2012.

Jiang, L.-Q., Feely, R. A., Wanninkhof, R., Greeley, D., Barbero, L., Alin, S., Carter, B. R., Pierrot, D., Featherstone, C., Hooper, J., Melrose, C., Monacci, N., Sharp, J. D., Shellito, S., Xu, Y.-Y., Kozyr, A., Byrne, R. H., Cai, W.-J., Cross, J., Johnson, G. C., Hales, B., Langdon, C., Mathis, J., Salisbury, J., and Townsend, D. W.: Coastal Ocean Data Analysis Product in North America (CODAP-NA) – an internally consistent data product for discrete inorganic carbon, oxygen, and nutrients on the North American ocean margins, Earth Syst. Sci. Data, 13, 2777–2799, https://doi.org/10.5194/essd-13-2777-2021, 2021.

Jung, J., Son, J. E., Lee, Y. K., Cho, K.-H., Lee, Y., Yang, E. J., Kang, S.-H., and Hur, J.: Tracing riverine dissolved organic carbon and its transport to the halocline layer in the Chukchi Sea (western Arctic Ocean) using humic-like fluorescence fingerprinting, Sci. Total Environ., 772, 145542, https://doi.org/10.1016/j.scitotenv.2021.145542, 2021.

Juranek, L. W., Feely, R. A., Peterson, W. T., Alin, S. R., Hales, B., Lee, K., Sabine, C. L., and Peterson, J.: A novel method for determination of aragonite saturation state on the continental shelf of central Oregon using multi-parameter relationships with hydrographic data, Geophys. Res. Lett., 36, L24601, https://doi.org/10.1029/2009GL040778, 2009.

Juranek, L. W., Feely, R. A., Gilbert, D., Freeland, H., and Miller, L. A.: Real-time estimation of pH and aragonite saturation state from Argo profiling floats: Prospects for an autonomous carbon observing strategy, Geophys. Res. Lett., 38, L17603, https://doi.org/10.1029/2011gl048580, 2011.

Koch, C. W., Cooper, L. W., Lalande, C., Brown, T. A., Frey, K. E., and Grebmeier, J. M.: Seasonal and latitudinal variations in sea ice algae deposition in the Northern Bering and Chukchi Seas determined by algal biomarkers, PLoS ONE, 15, e0231178, https://doi.org/10.1371/journal.pone.0231178, 2020.

Kroeker, K. J., Powell, C., and Donham, E. M.: Windows of vulnerability: Seasonal mismatches in exposure and resource identity determine ocean acidification's effect on a primary consumer at high latitude, Glob. Change Biol., 27, 1042–1051, https://doi.org/10.1111/gcb.15449, 2021.

Kuletz, K. J., Ferguson, M. C., Hurley, B., Gall, A. E., Labunski, E. A., and Morgan, T. C.: Seasonal spatial patterns in seabird and marine mammal distribution in the eastern Chukchi and western Beaufort seas: Identifying biologically important pelagic areas, Prog. Oceanogr., 136, 175–200, https://doi.org/10.1016/j.pocean.2015.05.012, 2015.

Lalande, C., Grebmeier, J. M., Hopcroft, R. R., and Danielson, S. L.: Annual cycle of export fluxes of biogenic matter near Hanna Shoal in the northeast Chukchi Sea, Deep-Sea Res. Pt. II, 177, 104730, https://doi.org/10.1016/j.dsr2.2020.104730, 2020.

Lalande, C., Grebmeier, J. M., McDonnell, A. M. P., Hopcroft, R. R., O'Daly, S., and Danielson, S. L.: Impact of a warm anomaly in the Pacific Arctic region derived from time-series export fluxes, PLOS ONE, 16, e0255837, https://doi.org/10.1371/journal.pone.0255837, 2021.

Lauvset, S. K., Lange, N., Tanhua, T., Bittig, H. C., Olsen, A., Kozyr, A., Álvarez, M., Becker, S., Brown, P. J., Carter, B. R., Cotrim da Cunha, L., Feely, R. A., van Heuven, S., Hoppema, M., Ishii, M., Jeansson, E., Jutterström, S., Jones, S. D., Karlsen, M. K., Lo Monaco, C., Michaelis, P., Murata, A., Pérez, F. F., Pfeil, B., Schirnick, C., Steinfeldt, R., Suzuki, T., Tilbrook, B., Velo, A., Wanninkhof, R., Woosley, R. J., and Key, R. M.: An updated version of the global interior ocean biogeochemical data product, GLODAPv2.2021, Earth Syst. Sci. Data, 13, 5565–5589, https://doi.org/10.5194/essd-13-5565-2021, 2021.

Lee, K., Kim, T.-W., Byrne, R. H., Millero, F. J., Feely, R. A., and Liu, Y.-M.: The universal ratio of boron to chlorinity for the North Pacific and North Atlantic oceans, Geochim. Cosmochim. Ac., 74, 1801–1811, https://doi.org/10.1016/j.gca.2009.12.027, 2010.

Lewis, E. and Wallace, D. W. R.: Program Developed for CO_2 System Calculations, ORNL/CDIAC-105, Carbon Dioxide Inf. Anal. Cent., Oak Ridge Natl. Lab., Oak Ridge, Tenn., 38 pp., https://salish-sea.pnnl.gov/media/ORNL-CDIAC-105.pdf (last access: 24 April 2019), 1998.

Lewis, K. M., van Dijken, G. L., and Arrigo, K. R.: Changes in phytoplankton concentration now drive increased Arctic Ocean primary production, Science, 369, 198–202, https://doi.org/10.1126/science.aay8380, 2020.

Li, B., Watanabe, Y. W., and Yamaguchi, A.: Spatiotemporal distribution of seawater pH in the North Pacific subpolar region by using the parameterization technique, J. Geophys. Res.-Oceans, 121, 3435–3449, https://doi.org/10.1002/2015JC011615, 2016.

Licker, R., Ekwurzel, B., Doney, S. C., Cooley, S. R., Lima, I. D., Heede, R., and Frumhoff, P. C.: Attributing ocean acidification to major carbon producers, Environ. Res. Lett., 14, 124060, https://doi.org/10.1088/1748-9326/ab5abc, 2019.

Lueker, T. J., Dickson, A. G., and Keeling, C. D.: Ocean pCO_2 calculated from dissolved inorganic carbon, alkalinity, and equations for K1 and K2: validation based on laboratory measurements of CO_2 in gas and seawater at equilibrium, Mar. Chem., 70, 105–119, https://doi.org/10.1016/S0304-4203(00)00022-0, 2000.

Mathis, J. T. and Questel, J. M.: Assessing seasonal changes in carbonate parameters across small spatial gradients in the Northeastern Chukchi Sea, Cont. Shelf Res., 67, 42–51, https://doi.org/10.1016/j.csr.2013.04.041, 2013.

Martz, T. R., Connery, J. G., and Johnson, K. S.: Testing the Honeywell Durafet for seawater pH applications, Limnol. Oceanogr. Meth., 8, 172–184, https://doi.org/10.4319/lom.2010.8.172, 2010.

McDougall, T. J. and Barker, P. M.: Getting started with TEOS-10 and the Gibbs Seawater (GSW) Oceanographic Toolbox, 28 pp., SCOR/IAPSO WG127, ISBN 978-0-646-55621-5, 2011.

Monacci, N. M., Cross, J. N., Pickart, R. S., Juranek, L. W., McRaven, L. T., and Becker, S.: Dissolved inorganic carbon (DIC) and total alkalinity (TA) and other hydrographic and chemical data collected from discrete sample and profile observations aboard the RV Sikuliaq Cruise SKQ202014S (EXPOCODE 33BI20201025) in the Bering and Chukchi Sea along transect lines in the Distributed Biological Observatory (DBO) from 2020-10-25 to 2020-11-11 (NCEI Accession 0252613), NOAA National Centers for Environmental Information [data set], https://doi.org/10.25921/pnsd-sv10, 2022.

Moore, S. E. and Stabeno, P. J.: Synthesis of Arctic Research (SOAR) in marine ecosystems of the Pacific Arctic, Prog. Oceanogr., 136, 1–11, https://doi.org/10.1016/j.pocean.2015.05.017, 2015.

Moore, S. E., Clarke, J. T., Okkonen, S. R., Grebmeier, J. M., Berchok, C. L., and Stafford, K. M.: Changes in gray whale phenology and distribution related to prey variability and ocean biophysics in the northern Bering and eastern Chukchi seas, PLOS ONE, 17, e0265934, https://doi.org/10.1371/journal.pone.0265934, 2022.

Mordy, C. W., Bell, S., Cokelet, E. D., Ladd, C., Lebon, G., Proctor, P., Stabeno, P., Strausz, D., Wisegarver, E., and Wood, K.: Seasonal and interannual variability of nitrate in the eastern Chukchi Sea: Transport and winter replenishment, Deep-Sea Res. Pt. II, 177, 104807, https://doi.org/10.1016/j.dsr2.2020.104807, 2020.

National Academies of Sciences, Engineering and Medicine: Valuing Climate Damages: Updating Estimation of the Social Cost of Carbon Dioxide, The National Academies Press, Washington DC, https://doi.org/10.17226/24651, 2017.

Newton, J. A., Feely, R. A., Jewett, E. B., Williamson, P., and Mathis, J.: Global ocean acidification observing network: requirements and governance plan, GOA-ON, Washington, 61 pp., https://www.iaea.org/sites/default/files/18/06/goa-on-second-edition-2015.pdf (last access: 18 January 2021), 2015.

Orr, J. C.: Recent and future changes in ocean carbonate chemistry, in: Ocean acidification, edited by: Gattuso, J.-P.

and Hansson, L., Oxford University Press, Oxford, 41–66, https://doi.org/10.1093/oso/9780199591091.003.0008, 2011.

Orr, J. C., Epitalon, J.-M., Dickson, A. G., and Gattuso, J.-P.: Routine uncertainty propagation for the marine carbon dioxide system, Mar. Chem., 207, 84–107, https://doi.org/10.1016/j.marchem.2018.10.006, 2018.

Orr, J. C., Kwiatkowski, L., and Pörtner, H. O.: Arctic Ocean annual high in pCO_2 could shift from winter to summer, Nature, 610, 94–100, https://doi.org/10.1038/s41586-022-05205-y, 2022.

Ouyang, Z., Collins, A., Li, Y., Qi, D., Arrigo, K. R., Zhuang, Y., Nishino, S., Humphreys, M. P., Kosugi, N., Murata, A., Kirchman, D. L., Chen, L., Chen, J., and Cai, W.-J.: Seasonal Water Mass Evolution and Non-Redfield Dynamics Enhance CO_2 Uptake in the Chukchi Sea, J. Geophys. Res.-Oceans, 127, e2021JC018326, https://doi.org/10.1029/2021JC018326, 2022.

Payne, C. M., Bianucci, L., van Dijken, G. L., and Arrigo, K. R.: Changes in Under-Ice Primary Production in the Chukchi Sea From 1988 to 2018, J. Geophys. Res.-Oceans, 126, e2021JC017483, https://doi.org/10.1029/2021JC017483, 2021.

Perez, F. F. and Fraga, F.: Association constant of fluoride and hydrogen ions in seawater, Mar. Chem., 21, 161–168, https://doi.org/10.1016/0304-4203(87)90036-3, 1987.

Pipko, I. I., Semiletov, I. P., Tishchenko, P. Y., Pugach, S. P., and Christensen, J. P.: Carbonate chemistry dynamics in Bering Strait and the Chukchi Sea, Prog. Oceanogr., 55, 77–94, https://doi.org/10.1016/S0079-6611(02)00071-X, 2002.

Qi, D., Chen, L., Chen, B., Gao, Z., Zhong, W., Feely, R. A., Anderson, L. G., Sun, H., Chen, J., Chen, M., Zhan, L., Zhang, Y., and Cai, W.-J.: Increase in acidifying water in the western Arctic Ocean, Nat. Clim. Change, 7, 195–199, https://doi.org/10.1038/nclimate3228, 2017.

Qi, D., Ouyang, Z., Chen, L., Wu, Y., Lei, R., Chen, B., Feely, R. A., Anderson, L. G., Zhong, W., Lin, H., Polukhin, A., Zhang, Y., Zhang, Y., Bi, H., Lin, X., Luo, Y., Zhuang, Y., He, J., Chen, J., and Cai, W. J.: Climate change drives rapid decadal acidification in the Arctic Ocean from 1994 to 2020, Science, 377, 1544–1550, https://doi.org/10.1126/science.abo0383, 2022a.

Qi, D., Wu, Y., Chen, L., Cai, W.-J., Ouyang, Z., Zhang, Y., Anderson, L. G., Feely, R. A., Zhuang, Y., Lin, H., Lei, R., and Bi, H.: Rapid acidification of the Arctic Chukchi Sea waters driven by anthropogenic forcing and biological carbon recycling, Geophys. Res. Lett., 49, e2021GL097246, https://doi.org/10.1029/2021GL097246, 2022b.

Raimondi, L., Matthews, J. B. R., Atamanchuck, D., Azetsu-Scott, K., and Wallace, D.: The internal consistency of the marine carbon dioxide system for high latitude shipboard and in situ monitoring, Mar. Chem., 213, 49–70, https://doi.org/10.1016/j.marchem.2019.03.001, 2019.

Rantanen, M., Karpechko, A. Y., Lipponen, A., Nordling, K., Hyvärinen, O., Ruosteenoja, K., Vihma, T., and Laaksonen, A.: The Arctic has warmed nearly four times faster than the globe since 1979, Commun. Earth Environ., 3, 1–10, https://doi.org/10.1038/s43247-022-00498-3, 2022.

Rheuban, J. E., Doney, S. C., McCorkle, D. C., and Jakuba, R. W.: Quantifying the Effects of Nutrient Enrichment and Freshwater Mixing on Coastal Ocean Acidification, J. Geophys. Res.-Oceans, 124, 9085–9100, https://doi.org/10.1029/2019JC015556, 2019.

Rysgaard, S., Glud, R. N., Sejr, M. K., Bendtsen, J., and Christensen, P. B.: Inorganic carbon transport during sea ice growth and decay: A carbon pump in polar seas, J. Geophys. Res., 112, C03016, https://doi.org/10.1029/2006JC003572, 2007.

Rysgaard, S., Glud, R. N., Lennert, K., Cooper, M., Halden, N., Leakey, R. J. G., Hawthorne, F. C., and Barber, D.: Ikaite crystals in melting sea ice – implications for pCO_2 and pH levels in Arctic surface waters, The Cryosphere, 6, 901–908, https://doi.org/10.5194/tc-6-901-2012, 2012.

Sakamoto, C. M., Johnson, K. S., and Coletti, L. J.: Improved algorithm for the computation of nitrate concentrations in seawater using an in situ ultraviolet spectrophotometer, Limnol. Oceanogr. Meth., 7, 132–143, https://doi.org/10.4319/lom.2009.7.132, 2009.

Sandy, S. J., Danielson, S. L., and Mahoney, A. R.: Automating the Acoustic Detection and Characterization of Sea Ice and Surface Waves, J. Mar. Sci. Eng., 10, 1577, https://doi.org/10.3390/jmse10111577, 2022.

Sarmiento, J. L. and Gruber, N.: Ocean Biogeochemical Dynamics, Princeton University Press, Princeton, NJ, 526 pp., ISBN 9780691017075, 2006.

Seabird: Application Note 31: Computing temperature and conductivity slope and offset correction coefficients from lab calibration and salinity bottle samples, https://my.hach.com/asset-get.download.jsa?id=54627861537, last access: 20 June 2016.

Seabird: Module 28. Advanced Biogeochemical Processing, https://www.seabird.com/cms-portals/seabird_com/cms/documents/training/Module28_Advanced_Biogeochem_Processing.pdf, last access: 30 May 2023.

Seferian, R.: CNRM-CERFACS CNRM-ESM2-1 model output prepared for CMIP6 AerChemMIP, Earth System Grid Federation, https://doi.org/10.22033/ESGF/CMIP6.1389, 2019.

Semiletov, I., Pipko, I., Gustafsson, Ö., Anderson, L. G., Sergienko, V., Pugach, S., Dudarev, O., Charkin, A., Gukov, A., Bröder, L., Andersson, A., Spivak, E., and Shakhova, N.: Acidification of East Siberian Arctic Shelf waters through addition of freshwater and terrestrial carbon, Nat. Geosci., 9, 361–365, https://doi.org/10.1038/ngeo2695, 2016.

Serreze, M. C. and Barry, R. G.: Processes and impacts of Arctic amplification: A research synthesis, Global Planet. Change, 77, 85–96, https://doi.org/10.1016/j.gloplacha.2011.03.004, 2011.

Serreze, M. C. and Francis, J. A.: The Arctic amplification debate, Climatic Change, 76, 241–264, https://doi.org/10.1007/s10584-005-9017-y, 2006.

Serreze, M. C., Crawford, A. D., Stroeve, J. C., Barrett, A. P., and Woodgate, R. A.: Variability, trends, and predictability of seasonal sea ice retreat and advance in the Chukchi Sea, J. Geophys. Res.-Oceans, 121, 7308–7325, https://doi.org/10.1002/2016JC011977, 2016.

Sharp, J. D., Pierrot, D., Humphreys, M. P., Epitalon, J.-M., Orr, J. C., Lewis, E. R., and Wallace, D. W. R.: CO2SYSv3 for MATLAB, Zenodo, https://doi.org/10.5281/zenodo.7552554, 2023.

Shu, Q., Wang, Q., Årthun, M., Wang, S., Song, Z., Zhang, M., and Qiao, F: Arctic Ocean Amplification in a warming climate in CMIP6 models, Sci. Adv., 8, eabn9755, https://doi.org/10.1126/sciadv.abn9755, 2022.

Stabeno, P. J., Mordy, C. W., and Sigler, M. F.: Seasonal patterns of near-bottom chlorophyll fluorescence in the eastern

Chukchi Sea: 2010–2019, Deep-Sea Res. Pt. II, 177, 104842, https://doi.org/10.1016/j.dsr2.2020.104842, 2020.

Stackpoole, S., Butman, D., Clow, D., Verdin, K., Gaglioti, B., and Striegl, R. G.: Carbon burial, transport, and emission from inland aquatic ecosystems in Alaska, USGS Prof. Pap., 1826, 159–188, https://doi.org/10.3133/pp1826, 2016.

Stackpoole, S. M., Butman, D., Clow, D. W., Verdin, K. L., Gaglioti, B. V., Genet, H., and Striegl, R. G.: Inland waters and their role in the carbon cycle of Alaska, Ecol. Appl., 27, 1403–1420, https://doi.org/10.1002/eap.1552, 2017.

Silvers, L., Blanton, C., McHugh, C., John, J. G., Radhakrishnan, A., Rand, K., Balaji, V., Dupuis, C., Durachta, J., Guo, H., Hemler, R., Lin, P., Nikonov, S., Paynter, D. J., Ploshay, J., Vahlenkamp, H., Wilson, C., Wyman, B., Robinson, T., Zeng, Y., and Zhao, M.: NOAA-GFDL GFDL-CM4 model output prepared for CMIP6 CFMIP, Earth System Grid Federation, https://doi.org/10.22033/ESGF/CMIP6.1641, 2018.

Stroeve, J. C., Serreze, M. C., Holland, M. M., Kay, J. E., Malanik, J., and Barrett, A. P.: The Arctic's rapidly shrinking sea ice cover: a research synthesis, Climatic Change, 110, 1005–1027, https://doi.org/10.1007/s10584-011-0101-1, 2011.

Stroeve, J. C., Markus, T., Boisvert, L., Miller, J., and Barrett, A.: Changes in Arctic melt season and implications for sea ice loss, Geophys. Res. Lett., 41, 1216–1225, https://doi.org/10.1002/2013GL058951, 2014.

Stumpp, M., Hu, M. Y., Melzner, F., Gutowska, M. A., Dorey, N., Himmerkus, N., Holtmann, W. C., Dupont, S. T., Thorndyke, M. C., and Bleich, M.: Acidified seawater impacts sea urchin larvae pH regulatory systems relevant for calcification, P. Natl. Acad. Sci. USA, 109, 18192–18197, https://doi.org/10.1073/pnas.1209174109, 2012.

Sulpis, O., Lauvset, S. K., and Hagens, M.: Current estimates of K_1^* and K_2^* appear inconsistent with measured CO_2 system parameters in cold oceanic regions, Ocean Sci., 16, 847–862, https://doi.org/10.5194/os-16-847-2020, 2020.

Thomsen, J., Casties, I., Pansch, C., Körtzinger, A., and Melzner, F.: Food availability outweighs ocean acidification effects in juvenile Mytilus edulis: laboratory and field experiments, Glob. Change Biol., 19, 1017–1027, https://doi.org/10.1111/gcb.12109, 2013.

Thor, P. and Dupont, S.: Transgenerational effects alleviate severe fecundity loss during ocean acidification in a ubiquitous planktonic copepod, Glob. Change Biol., 21, 2261–2271, https://doi.org/10.1111/gcb.12815, 2015.

Tian, F., Pickart, R. S., Lin, P., Pacini, A., Moore, G. W. K., Stabeno, P., Weingartner, T., Itoh, M., Kikuchi, T., Dobbins, E., and Bell, S.: Mean and seasonal circulation of the eastern Chukchi Sea from moored timeseries in 2013–2014, J. Geophys. Res.-Oceans, 126, e2020JC016863, https://doi.org/10.1029/2020JC016863, 2021.

Tunnicliffe, V., Davies, K. T. A., Butterfield, D. A., Embley, R. W., Rose, J. W., and Chadwick Jr., W. W.: Survival of mussels in extremely acidic waters on a submarine volcano, Nat. Geosci., 2, 344–348, https://doi.org/10.1038/ngeo500, 2009.

Van Straalen, M. N.: Peer Reviewed: Ecotoxicology Becomes Stress Ecology, Environ. Sci. Technol., 37, 324A–330A, https://doi.org/10.1021/es0325720, 2003.

Vargas, C. A., Lagos, N. A., Lardies, M. A., Duarte, C., Manríquez, P. H., Aguilera, V. M., Broitman, B., Widdicombe, S., and Dupont, S.: Species-specific responses to ocean acidification should account for local adaptation and adaptive plasticity, Nat. Ecol. Evol., 1, 0084, https://doi.org/10.1038/s41559-017-0084, 2017.

Vargas, C. A., Cuevas, L. A., Broitman, B. R., San Martin, V. A., Lagos, N. A., Gaitán-Espitia, J. D., and Dupont, S.: Upper environmental pCO_2 drives sensitivity to ocean acidification in marine invertebrates, Nat. Clim. Change, 12, 200–207, https://doi.org/10.1038/s41558-021-01269-2, 2022.

Ventura, A., Schulz, S., and Dupont, S.: Maintained larval growth in mussel larvae exposed to acidified under-saturated seawater, Sci. Rep., 6, 23728, https://doi.org/10.1038/srep23728, 2016.

Vergara-Jara, M. J., DeGrandpre, M. D., Torres, R., Beatty, C. M., Cuevas, L. A., Alarcón, E., and Iriarte, J. L: Seasonal Changes in Carbonate Saturation State and Air-Sea CO_2 Fluxes During an Annual Cycle in a Stratified-Temperate Fjord (Reloncaví Fjord, Chilean Patagonia), J. Geophys. Res.-Biogeo., 124, 2851–2865, https://doi.org/10.1029/2019JG005028, 2019.

Watanabe, Y. W., Li, B. F., Yamasaki, R., Yunoki, S., Imai, K., Hosoda, S., and Nakano, Y.: Spatiotemporal changes of ocean carbon species in the western North Pacific using parameterization technique, J. Oceanogr., 76, 155–167, https://doi.org/10.1007/s10872-019-00532-7, 2020.

Williams, N. L., Juranek, L. W., Johnson, K. S., Feely, R. A., Riser, S. C., Talley, L. D., Russell, J. L., Sarmiento, J. L., and Wanninkhof, R.: Empirical algorithms to estimate water column pH in the Southern Ocean, Geophys. Res. Lett., 43, 3415–3422, https://doi.org/10.1002/2016GL068539, 2016.

Wieners, K.-H., Giorgetta, M., Jungclaus, J., Reick, C., Esch, M., Bittner, M., Legutke, S., Schupfner, M., Wachsmann, F., Gayler, V., Haak, H., de Vrese, P., Raddatz, T., Mauritsen, T., von Storch, J.-S., Behrens, J., Brovkin, V., Claussen, M., Crueger, T., Fast, I., Fiedler, S., Hagemann, S., Hohenegger, C., Jahns, T., Kloster, S., Kinne, S., Lasslop, G., Kornblueh, L., Marotzke, J., Matei, D., Meraner, K., Mikolajewicz, U., Modali, K., Müller, W., Nabel, J., Notz, D., Peters-von Gehlen, K., Pincus, R., Pohlmann, H., Pongratz, J., Rast, S., Schmidt, H., Schnur, R., Schulzweida, U., Six, K., Stevens, B., Voigt, A., and Roeckner, E.: MPI-M MPI-ESM1.2-LR model output prepared for CMIP6 CMIP historical, Earth System Grid Federation, https://doi.org/10.22033/ESGF/CMIP6.6595, 2019.

Wolf-Gladrow, D. A., Zeebe, R. E., Klaas, C., Körtzinger, A., and Dickson, A. G.: Total alkalinity: The explicit conservative expression and its application to biogeochemical processes, Mar. Chem., 106, 287–300, https://doi.org/10.1016/j.marchem.2007.01.006, 2007.

Wood, K. R., Bond, N. A., Danielson, S. L., Overland, J. E., Salo, S. A., Stabeno, P. J., and Whitefield, J.: A decade of environmental change in the Pacific Arctic region, Prog. Oceanogr., 136, 12–31, https://doi.org/10.1016/j.pocean.2015.05.005, 2015.

Woosley, R. J.: Evaluation of the temperature dependence of dissociation constants for the marine carbon system using pH and certified reference materials, Mar. Chem., 229, 103914, https://doi.org/10.1016/j.marchem.2020.103914, 2021.

Woosley, R. J. and Millero, F. J.: Freshening of the western Arctic negates anthropogenic carbon uptake potential, Limnol. Oceanogr., 65, 1834–1846, https://doi.org/10.1002/lno.11421, 2020.

Woosley, R. J., Millero, F. J., and Takahashi, T.: Internal consistency of the inorganic carbon system in the Arctic Ocean, Limnol. Oceanogr. Meth., 15, 887–896, https://doi.org/10.1002/lom3.10208, 2017.

Yamamoto-Kawai, M., McLaughlin, F. A., Carmack, E. C., Nishino, S., and Shimada, K.: Aragonite undersaturation in the Arctic Ocean: effects of ocean acidification and sea ice melt, Science, 326, 1098–1100, https://doi.org/10.1126/science.1174190, 2009.

Yamamoto-Kawai, M., Mifune, T., Kikuchi, T., and Nishino, S.: Seasonal variation of $CaCO_3$ saturation state in bottom water of a biological hotspot in the Chukchi Sea, Arctic Ocean, Biogeosciences, 13, 6155–6169, https://doi.org/10.5194/bg-13-6155-2016, 2016.